Volume 16
Number 35
21 September 2025
Pages 3889-3988

Polymer Chemistry

rsc.li/polymers

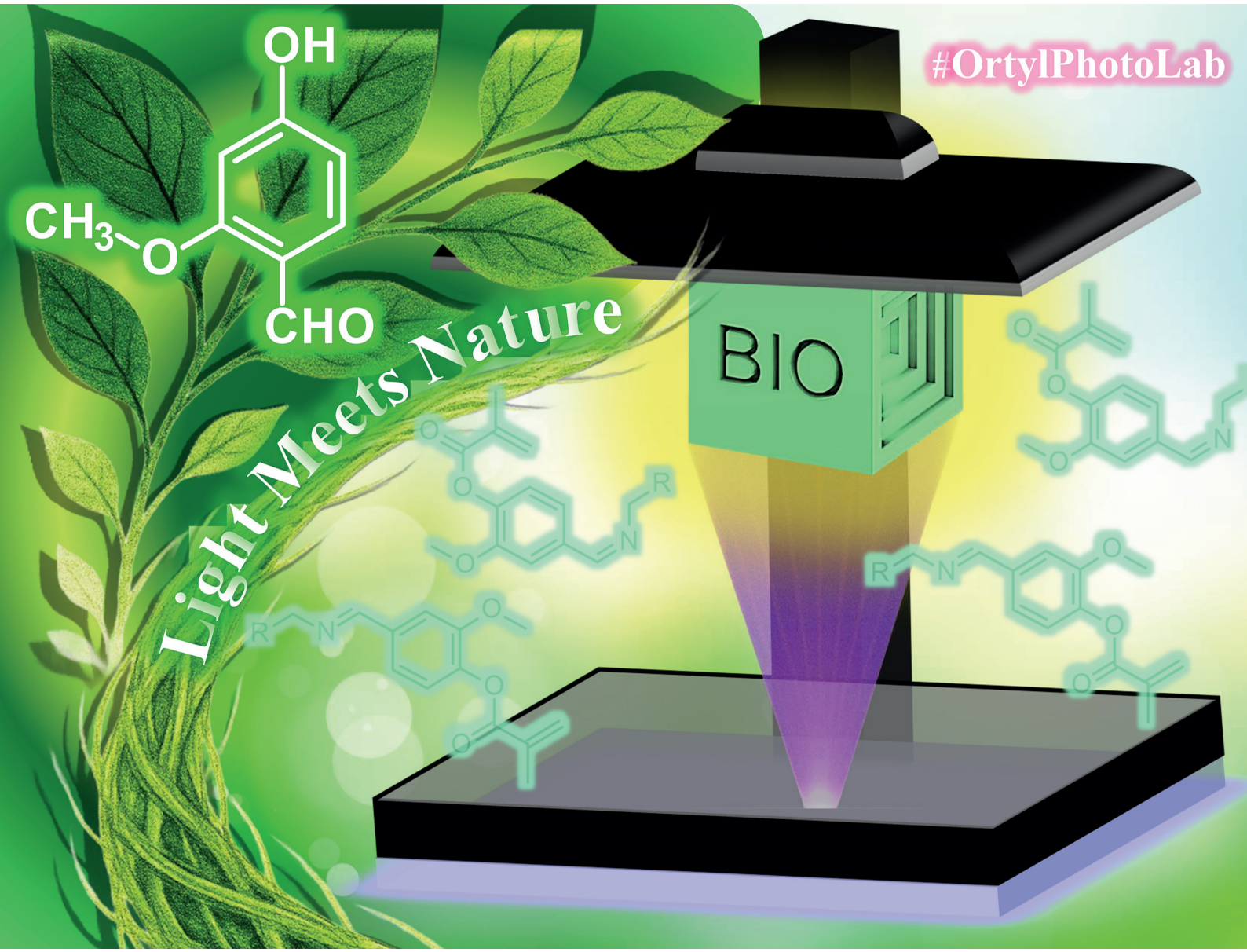

ISSN 1759-9962

ROYAL SOCIETY OF CHEMISTRY

PAPER
Emrah Çakmakçi, Joanna Ortyl *et al.*
A thiol-functional amine synergist as a co-initiator for DLP 3D printing applications

15 YEARS ANNIVERSARY

Polymer Chemistry

ROYAL SOCIETY OF CHEMISTRY

PAPER

View Article Online
View Journal | View Issue

Cite this: *Polym. Chem.*, 2025, **16**, 3895

A thiol-functional amine synergist as a co-initiator for DLP 3D printing applications

Magdalena Jankowska,[a] Ozge Ozukanar,[b] Emrah Çakmakçi *[c] and Joanna Ortyl *[d,e,f]

Received 17th June 2025,
Accepted 6th August 2025

DOI: 10.1039/d5py00603a

rsc.li/polymers

This article describes a newly synthesized thiol-functional amine synergist and its application as a co-initiator in two-component photoinitiating systems to initiate radical photopolymerization utilizing light sources in the ultraviolet and visible ranges. For this purpose, various investigations have been carried out to explore the spectroscopic properties of the newly synthesized amine and its influence on the kinetic parameters. Absorbance, photolysis, and electrochemical investigations were conducted, and kinetic measurements were performed using Fourier transform infrared spectroscopy. The final research stage involved application studies related to the use of amines in light-initiated 3D printing to obtain spatial structures as well as silica polymer nanocomposites. Additionally, an innovative aspect of this work is the synthesis and application of the dimer diamine-vanillin dimethacrylate monomer (DVDMA) in 3D printing. DVDMA, a bio-based monomer containing imine linkages, is readily cleavable under acidic conditions, thereby contributing to the degradation of 3D-printed parts.

1. Introduction

Currently, photopolymerization processes, and consequently, 3D printing in light-initiated technologies, are used in biomedical engineering,[1–6] medicine,[7–12] and dentistry.[13–16] Additive manufacturing utilizing DLP (digital light processing) technology allows three-dimensional structures with excellent precision to be obtained.[17–19] DLP 3D printing has become very popular owing to its ability to produce high-resolution materials and perfect surface finishes, which are extremely important in applications that require very high-quality materials.[20–22] DLP 3D printing, and consequently photopolymerization processes, are becoming increasingly popular owing to the high availability of monomers that polymerize according to the radical[23–25] and cationic[26–31] mechanism.

The crucial factor determining the effective photopolymerization process during DLP printing is the proper selection of initiating system components.[32] The initiator should completely or partially absorb the radiation emitted by the 3D printer projector (typically, λ = 405 nm).[33] The appropriate photoinitiator employed in the composition undergoing polymerization absorbs the radiation emitted by the light source and, under its influence, is broken down into radicals or ions (cations or anions), which in turn initiate the polymerization process. Initiation systems often include various amines[34,35] such as *N*,*N*-dimethyl-*p*-toluidine, 2-ethyl-dimethylbenzoate, and *N*-phenylglycine. The amines used in the initiator systems significantly accelerate the photopolymerization process, which is very important from an application point of view because it allows a significant reduction in the exposure time of individual layers during the 3D printing process. Shortening the exposure time reduces the duration of the printing process, resulting in lower costs. The selection of suitable monomers for photocurable resins is also significant as it determines the properties of the resulting material.[36–40] The monomers employed affected the mechanical parameters. The appropriate selection of input materials for the 3D printing process allows the fabrication of materials with specific properties tailored to unique applications. Therefore, materials with low polymerization shrinkage, high strength, and low cytotoxicity are obtained.

There is a growing trend towards the use of bio-based monomers and polymers in several applications, including 3D printing and photocuring, owing to the environmental issues associated with petroleum-derived polymers.[41–44] To efficiently design and synthesize bio-based monomers, one should consider the principles of green chemistry (GC), which was put

[a]*Cracow University of Technology, Faculty of Chemical Engineering and Technology, Department of Biotechnology and Physical Chemistry, CUT Doctoral School, Cracow, Poland*
[b]*Department of Chemistry, Istanbul Technical University, 34469 Istanbul, Türkiye*
[c]*Department of Chemistry, Marmara University, 34722 Istanbul, Türkiye. E-mail: emrah.cakmakci@marmara.edu.tr*
[d]*Cracow University of Technology, Faculty of Chemical Engineering and Technology, Department of Biotechnology and Physical Chemistry, Cracow, Poland. E-mail: jortyl@pk.edu.pl*
[e]*Photo HiTech Ltd, Bobrzynskiego 14, 30-348 Cracow, Poland*
[f]*Photo4Chem Lea 114, 30-133 Cracow, Poland*

forward by Paul Anastas in 1998 as an outcome of the approaches to resolve the problems of the depletion of petroleum resources and increasing environmental pollution.[45] According to the GC principles, the utilization of renewable feedstocks is of great importance. GC also emphasizes that materials should be designed for degradation. Therefore, several monomers have been prepared in recent years for photocuring and 3D-printing by taking these principles into account.[46–52] Herein, a monomer with a high bio-based content was synthesized using vanillin and the diamine dimer. The new monomer prepared in this study contains imine linkages that can be easily degraded under acidic conditions.

The search, design, and synthesis of new materials dedicated to DLP 3D printing is a major challenge and a focus area for many researchers involved in photopolymerization processes. This article presents newly synthesized materials dedicated to photopolymerization and their application in DLP 3D printing. The subject of this article is a newly synthesized diamine–vanillin dimethacrylate monomer and amine synergist AS. The effect of the addition of the AS compound on the radical photopolymerization kinetics was investigated. The effect of AS on the oxygen inhibition characteristics of photopolymerization processes that proceed according to the radical mechanism was also analyzed. The final stage of this research was an application study related to the utilization of the newly synthesized compounds in additive manufacturing using the DLP technique, which represents a promising approach in terms of suitability for further applications related to biomedical engineering.

2. Experimental

2.1. Materials

The newly synthesized amine synergist AS was employed as an amine co-initiator in the radical photopolymerization process; the synthesis description and scheme are presented in the supplement in the chapter titled "Amine synergist", and spectra confirming the structure of the amine are presented in Fig. S1–S4. Ethyl 4-dimethylaminobenzoate (EDB; Alfa Aesar) was used as the amine reference. The following compounds were used as commercial initiators: bis-(4-*t*-butylphenyl)iodonium hexafluorophosphate (IOD; Lambson), diphenyliodonium hexafluorophosphate (HIP; Alfa Aesar), (2,4,6-trimethyl benzoyl) phosphine oxide (TPO; Allnex), and (7-methoxy-4-methylcoumarin-3-yl)phenyliodonium hexafluorophosphate (7MP). The structures of all the photoinitiating system components are shown in Fig. 1.

The monomers chosen for the kinetics of the photopolymerization process and 3D printing experiments were trimethylolpropane triacrylate (TMPTA, Sigma Aldrich), 1,6-hexanediol diacrylate (HDDA, Sigma Aldrich), diurethane dimethacrylate, a mixture of isomers (UDMA, Sigma Aldrich), and the newly synthesized biobased monomer diamine–vanillin dimethacrylate. The synthesis description of the diamine–vanillin dimethacrylate monomer and the synthesis scheme

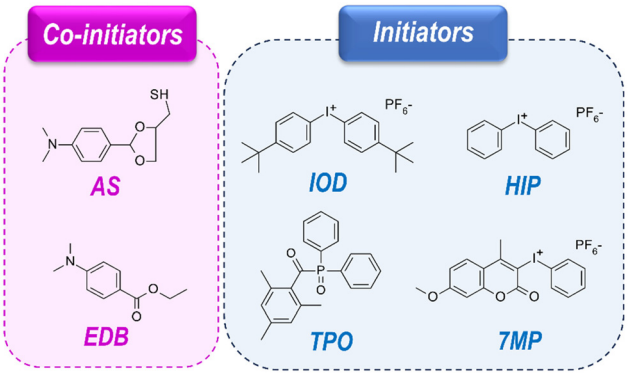

Fig. 1 The structures of photoinitiating system components.

are presented in the Supplement in the chapter titled "Biobased monomer", and the spectra confirming the structure of the obtained monomer are presented in Fig. S5–S8. The structure of the monomer was validated using NMR and FT-IR. The monomer structures employed to investigate radical photopolymerization kinetics are shown in Fig. 2.

Silicon dioxide was utilized to obtain photocurable polymer nanocomposites (nanoparticle size 10–20 nm; Sigma Aldrich).

2.2. Characterization methods

2.2.1. Spectroscopic measurements. To determine the spectroscopic properties (absorbance and photolysis measurements) of the individual components of the initiating system, a Cary 60 UV-VIS spectrophotometer (Agilent Technologies) with a wide spectral range of 190–1100 nm equipped with a xenon flash lamp (80 Hz) was employed. Solutions of the investigated components of the initiating system in acetonitrile at a concentration of 8.4×10^{-5} mol dm^{-3} were placed in a quartz cuvette with an optical path length of 1 cm. The obtained raw

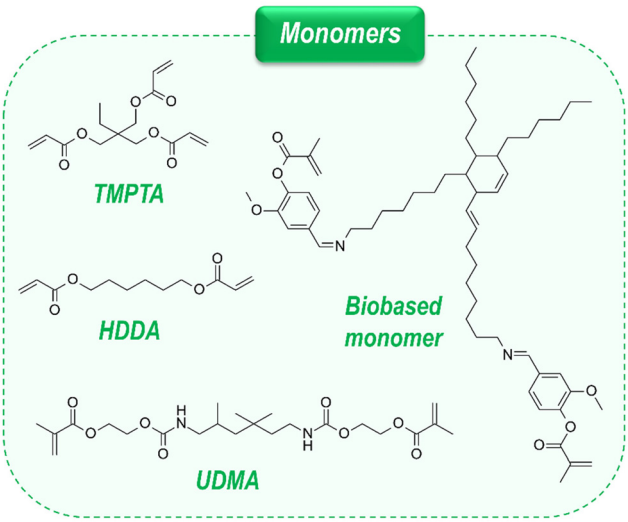

Fig. 2 The monomer structures utilized for kinetic research and 3D printing experiments.

results were converted and presented as the dependence of the molar extinction coefficient on the wavelength, and the following formula was used:

$$\varepsilon = \frac{A}{l \times c} \quad (1)$$

where ε is the molar extinction coefficient [mol^{-1} dm^3 cm^{-1}], A is the absorbance, l is the optical path [cm], and c is the sample concentration [mol dm^{-3}]. Photostability measurements were performed for the newly synthesized amine synergist using a solution of the same concentration as that used for the absorbance measurements. Photolysis was performed using various light sources in the ultraviolet range. The following diodes were applied as light sources: λ_{max} = 300 nm (M300L4 Thorlabs; the light intensity on the photolysis solution was 14.98 mW cm^{-2}), λ_{max} = 340 nm (M340L4 Thorlabs, the light intensity on the photolysis solution was 14.98 mW cm^{-2}), and λ_{max} = 365 nm (M365L3 Thorlabs, the light intensity on the photolysis solution was 14.98 mW cm^{-2}).

2.2.2. Oxidation potential measurements. The oxidation potential of the AS compound (E_{ox} *vs.* Ag/AgCl), playing the role of the co-initiator, was measured using cyclic voltammetry. For this purpose, an electrochemical analyzer M161 and an electrode stand M164 (MTM-ANKO, Poland) were used with a standard three-electrode cell. Tetrabutylammonium hexafluorophosphate (0.1 M) (Sigma Aldrich) was employed as the basic electrolyte. A platinum plate was used as the auxiliary electrode, a silver electrode (Ag/AgCl) was used as the reference electrode, and a glassy carbon electrode was applied as the working electrode. Voltammetry was performed at a scan rate of 100 mV s^{-1}; ferrocene was used as a standard, and the potentials were determined from the half-peak potentials.

2.2.3. Photopolymerization kinetics investigation. Fourier transform infrared spectroscopy (FTIR) was employed to verify the effect of the amine synergist additive on the kinetics of the photopolymerization process. An FT/IR-6700 spectrometer (Jasco) equipped with a special holder dedicated to measuring the photopolymerization kinetics was utilized. The measurements were conducted in a thermostatic chamber where the temperature was maintained at 25 °C during all measurements. The light source was a diode with λ_{max} = 340 nm and λ_{max} = 405 nm. The optical fiber end was 2.1 cm away from the photopolymerizing composition. The conversion was calculated based on the band area (A) characteristic of acrylates (υ = 1635 cm^{-1} for acrylic C=C bond oscillation).[53] The following formula[54–56] was employed to determine the conversion of the acrylate monomer:

$$\text{Conversion} = \left(1 - \frac{A_{\text{after polymerization}}}{A_{\text{before polymerization}}}\right) \times 100[\%] \quad (2)$$

The preparation of photocurable resins for radical photopolymerization consists of dissolving the initiator system in the radical monomer TMPTA or in a mixture of monomers that polymerize according to the radical mechanism. Measurements were carried out between fragments of a polypropylene film, which allowed anaerobic conditions. The photocurable resin was applied to the film in such a way as to obtain an absorbance value of 1.2 for the maximum observed acrylate-specific band. In addition, to examine the effect of atmospheric oxygen on the photopolymerizing composition with the addition of an amine synergist, measurements were performed on a barium fluoride-made pastille.

2.2.4. Measurements of thermal stability of AS and photocurable resins with AS addition. Thermal stability measurements were carried out using differential scanning calorimetry (DSC) on a Photo-DSC 204 F1 Phoenix calorimeter (from Netzsch-Gerätebau GmbH, Germany), equipped with a thermal attachment. The thermal stability of the AS compound was measured using a special attachment dedicated to thermal measurements. The measurement was carried out in a closed crucible (aluminum lid pierced) under a nitrogen flow of 50 ml min^{-1}. The measurement consisted of heating the compound in the closed crucible to 200 °C and then cooling the measurement system. An empty crucible was used as a reference. Measurements of compositions containing different weight concentrations of AS (0%, 1%, 2% and 5%) in a monomer mixture (HDDA/UDMA/biobased monomer) included heating the system to 200 °C, followed by cooling the measurement system. The monomer mixture (without the addition of TPO and AS) was applied as a reference.

2.2.5. Additive manufacturing experiments. 3D printing was performed with a Lumen X+™ printer (CellInk Inc.), which works on DLP technology; the light source was a projector that emits maximum energy at a wavelength of λ = 405 nm. The intensity of light incident on the printed surface object was 1.99–9.95 mW cm^{-2}. The light intensities were measured using a PM160 measuring device (Si Sensor Power Meter, ThorLabs). 3D printing experiments were performed for resin polymerization according to the radical mechanism, together with the amine synergist, to investigate the effect of the addition of the newly synthesized co-initiator on 3D printing parameters, as well as on the quality of the obtained three-dimensional structures. All 3D models utilized for printing were designed using Fusion 360 software (AutoDesk) in stl. format. Jacob's working curve test was employed to determine the critical energy, E_c, and light penetration depth, D_p, using the following formula:[57–59]

$$C_d = D_p \ln\left[\frac{E_0}{E_c}\right] \quad (3)$$

where C_d is the thickness of the cured layer [μm] and E_0 is the light energy at the surface [mJ cm^{-2}].

The models utilized for the 3D printing experiments are shown in Fig. 3. Fig. 3a illustrates the design of a slice dedicated to performing Jacob's working curve test. Fig. 3b and c show the 2D and 3D projects designed for 3D printing utilizing photocurable resins.

2.2.6. Investigation of viscosity properties of resins dedicated to photocurable 3D printing of polymer composites. A modular compact Rheometer MCR302 (Anton Paar, Ashland,

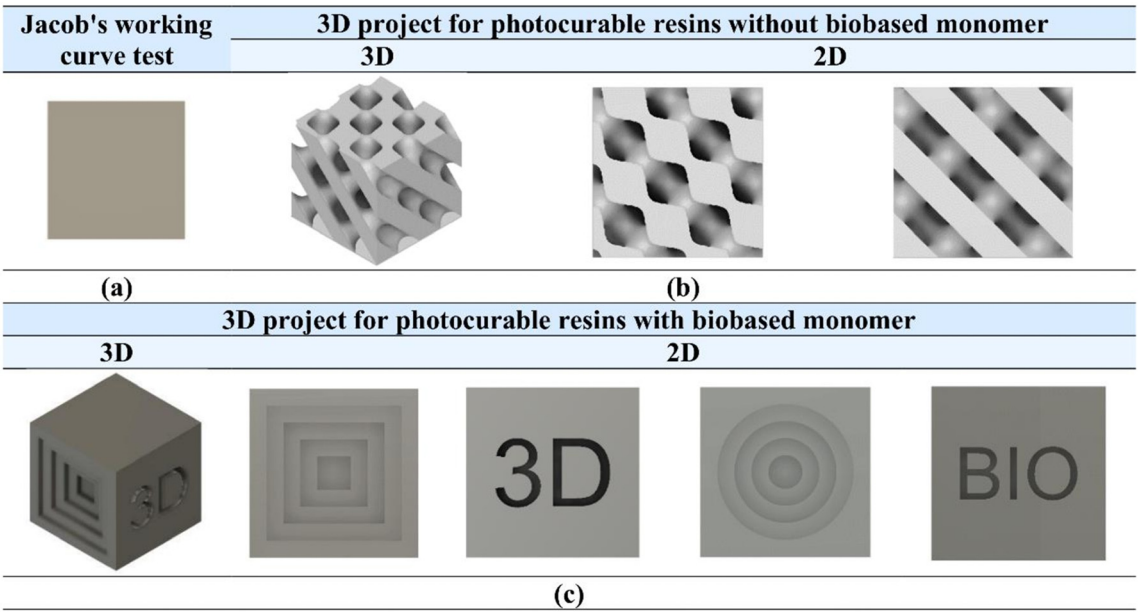

Fig. 3 Models utilized for the 3D DLP printing experiments: (a) Jacob's working curve test slice design, (b) cube model applied to DLP 3D printing with photocurable resins without the addition of biobased monomer, (c) cube model utilized for DLP 3D printing with photocurable resins with biobased monomer.

VA, USA) was utilized to investigate the viscosity properties of the resins for 3D printing. The experiments were conducted at 25 °C. Each measurement lasted 550 s. The measurement gap between the spindle and the platform was 0.1 mm. A PP25 measuring spindle was employed for viscosity measurements. The RheoCompass software was set to a variable head speed (shear rate) ranging from 1 s^{-1} to 100 s^{-1}.

2.2.7. Visualization of printed spatial structures

2.2.7.1. Optical microscopy analysis. An OLYMPUS DSX1000 optical microscope was employed for the optical imaging of the 3D prints. The images were captured with an objective that guarantees a three-fold zoom of the composite structure printed by applying 3D DLP technology. DSX software, dedicated to the analysis of 3D structures, was utilized to obtain microscopic images.

2.2.7.2. SEM analysis. To analyze the surface quality of the obtained prints, a high-resolution scanning electron microscope Apreo 2 S LoVac (Thermo Fisher Scientific) equipped with X-ray dispersive spectrometry (EDS) UltraDry (Thermo Fisher Scientific) and octane element (EDAX Ametek GmbH) detectors was employed. The imaging of prints coated with a thin layer of gold was performed at an accelerating voltage of 2.0 kV and an electron beam current of 0.4 nA.

2.2.7.3. Gel content. The gel content of the selected photocured compositions was determined *via* Soxhlet extraction, using acetone as the solvent. The details and gel content calculations have been described elsewhere.[60,61]

2.2.7.4. Contact Angle. The water contact angles (WCA) of the photosets were determined using a Kruss tensiometer (Easy Drop DSA-2). Measurements were performed using 3–5 μL drops of distilled water. At least three measurements were taken for each sample, and the average was recorded.

2.2.7.5. Optical properties. Transmission spectra of the photosets were obtained using a Shimadzu 3100 UV-vis-NIR spectrometer.

2.2.7.6. Thermogravimetric analyses. Thermogravimetric analysis (TGA) of the photosets was performed using a PerkinElmer thermogravimetric analyzer (Pyris 1 TGA model). Samples were run from 30 to 600 °C at a heating rate of 20 °C min^{-1} under a nitrogen atmosphere.

3. Results and discussion

3.1. Spectroscopic and electrochemical properties of the amine synergist and other components of initiating systems

Absorbance analyses were conducted to understand the spectroscopic characteristics of the initiating system components. Absorbance measurements of the commercial cationic photoinitiators based on iodonium salts: IOD (bis-(4-*t*-butylphenyl) iodonium hexafluorophosphate), HIP (diphenyliodonium hexafluorophosphate), and 7MP ((7-methoxy-4-methylcoumarin-3-yl)phenyliodonium hexafluorophosphate) and amine compounds as co-initiators (commercially available amine EDB (ethyl 4-dimethylaminobenzoate) and the newly synthesized co-initiator AS for initiating radical photopolymerization) were performed. The measurements demonstrated that the amine synergist AS absorbs radiation in the ultraviolet range, reaching a wavelength of λ = 370 nm, whereas the absorption spectrum of the commercial co-

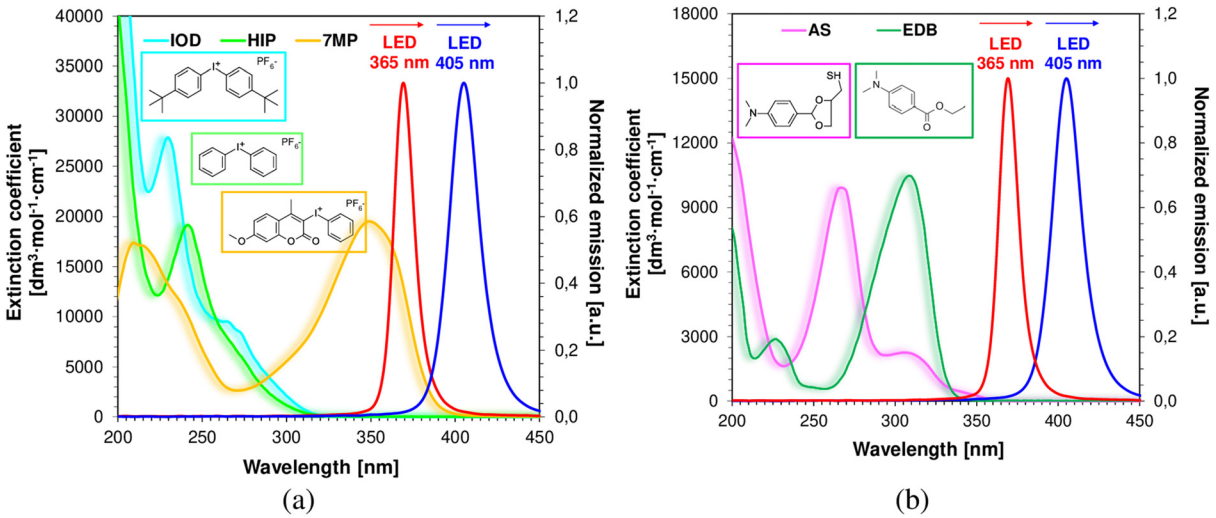

Fig. 4 (a and b) Comparison of the absorption characteristics of (a) iodonium salt-based photoinitiators: IOD, HIP and 7MP used for the photopolymerization process and (b) amine co-initiators AS and EDB with the emission spectra of UV- and VisLED-type light sources.

initiator EDB reaches λ = 350 nm, which already suggests an advantage of AS over EDB, as it allows an increase in the range of light sources used for the photopolymerization process. Moreover, the absorption characteristics of the initiators, which were subsequently applied to initiate the radical photopolymerization process in combination with an amine co-initiator, were also compared. As shown in Fig. 4a, commercially available cationic photoinitiators based on the iodonium salt IOD and HIP absorb irradiation up to approximately 320 nm. However, the absorption of the cationic initiator, 7MP, extended to the visible range. The absorbance spectra of all initiators/co-initiators employed to initiate the radical photopolymerization process are shown in Fig. 4a and b.

The molar extinction coefficients and absorption maxima are summarized in Table 1.

In addition, the photostability of the amine synergist AS in acetonitrile was measured to check the stability of the newly synthesized compound under different ultraviolet light sources (λ = 300 nm, λ = 340 nm, and 365 nm). Research using light sources with λ = 340 nm and λ = 365 nm confirmed that the compound was stable. The photolysis characteristics of the AS compound are presented in the SI (Fig. S9a–S9c). Moreover, to confirm the feasibility of employing the amine synergist AS as a co-initiator in two-component initiator systems for initiating radical photopolymerization, its oxidation potential was compared to that of the commonly used EDB co-initiator. Electrochemical tests were performed on the amine synergists using cyclic voltammetry. Studies have shown that the oxidation potential of amine synergists is 792 mV, whereas literature data show that the oxidation potential of EDB is 1058 mV (*vs.* Ag/AgCl).[62] The cyclic voltammogram curves of the oxidation of the amine synergist AS in acetonitrile are shown in the SI (Fig. S10).

3.2. Effect of amine synergist addition on radical photopolymerization kinetics under both aerobic and oxygen-limited conditions

The first stage of kinetic studies involved checking the effect of the amine synergist additive on radical photopolymerization kinetics under different conditions, that is, under aerobic and atmospheric oxygen-limited conditions. The composition of the monomer mixture was optimized for further kinetic experiments and for light-initiated 3D printing. For these experiments, the synthesized biobased monomer containing imine linkages (DVDMA), displaying degradability under acidic conditions or leading to dynamic covalent networks, was

Table 1 Spectroscopic characterization of commercial cationic photoinitiators based on an iodonium salt and amine compounds as co-initiators

Compound	$\lambda^{*}_{\text{max-ab}}$ [nm]	$\varepsilon^{*}_{@\lambda\text{max-ab}}$	$\varepsilon@\lambda_{340\text{ nm}}$	$\varepsilon@\lambda_{365\text{ nm}}$	$\varepsilon@\lambda_{405\text{ nm}}$
Commercial cationic photoinitiators based on an iodonium salt					
IOD	241	21 695	—	—	—
HIP	229	14 566	—	—	—
7MP	350	22 384	19 645	18 197	47
Amine co-initiators					
AS	340	450	450	18	—
EDB	309	10 464	132	—	—

$\lambda^{*}_{\text{max-ab}}$ – the wavelength corresponding to the absorption maximum for the longest wavelength band [nm]. $\varepsilon^{*}_{@\lambda\text{max-ab}}$ – extinction coefficient at $\lambda_{\text{max–ab}}$.

employed. Various amounts of this monomer (0, 10, 20, 30, and 40% by weight) were added to the UDMA/HDDA (60/40 w/w) formulation, replacing UDMA. The commercially available TPO radical initiator (1% w/w) was used as the photoinitiator. The initiator was weighed in relation to the monomer matrix. The precise compositions of the resins investigated are listed in Table 2. Measurements were performed under oxygen-limited conditions. For the measurements, a Vis-LED emitting radiation with a wavelength of λ = 405 nm was applied, where the intensity of the light incident on the examined sample was 5.58 mW cm^{-2}.

Investigations of the effect of biobased monomer addition on kinetic parameters showed that functional group conversion first increased with 10% and 20% biobased monomer addition and then started to decrease (Fig. 5a). The functional group conversion was calculated based on the disappearance of the band characteristic of acrylate groups – υ = 1635 cm^{-1} (Fig. 5b). When the concentration of the newly synthesized monomer was 40%, a dramatic decrease in conversion was observed compared to a smaller amount of biobased monomer-containing formulations (≥30%). This was attributed to the increased viscosity of the formulation. The formulation with the composition UDMA : HDDA : biobased monomer 40 : 40 : 20 was selected for subsequent experiments related to the effect of atmospheric oxygen on the photopolymerizing formulation and 3D printing experiments because it had the highest conversion of acrylate groups (C = 88%), the highest value of the dC/dt kinetic curve slope (dC/dt = 4.37 s^{-1}, Fig. 5c), and a short induction time (2.51 s, Fig. 5c) (Table 3).

Table 3 demonstrates the effect of biobased monomer addition on the conversion of functional groups, slope of the kinetic curve, and induction time during the measurement of the radical photopolymerization process kinetics.

The primary kinetic research stage allowed optimization of the monomer composition of the photocurable resin. Subsequently, the effects of the amine synergist additives (0, 1, 2, and 5% w/w) on the kinetics of the radical photopolymerization process were examined (Table 4). The amine synergist, like the initiator, was weighed relative to the monomer matrix. Initially, the tests were conducted under anaerobic conditions, where a drop of the photopolymerizing composition was applied between two pieces of polypropylene film. The measurements involved a Vis-LED emitting radiation with a wavelength of λ = 405 nm, where the intensity of the

Table 2 Formulation of photocurable resins polymerized by the radical mechanism based on the UDMA/HDDA/biobased monomer and the TPO initiator

Resin	UDMA (w/w)	HDDA (w/w)	Biobased monomer (w/w)	TPO (w/w)
Resin-0% BIO-TPO	60%	40%	0%	1%
Resin-10% BIO-TPO	50%		10%	
Resin-20% BIO-TPO	40%		20%	
Resin-30% BIO-TPO	30%		30%	
Resin-40% BIO-TPO	20%		40%	

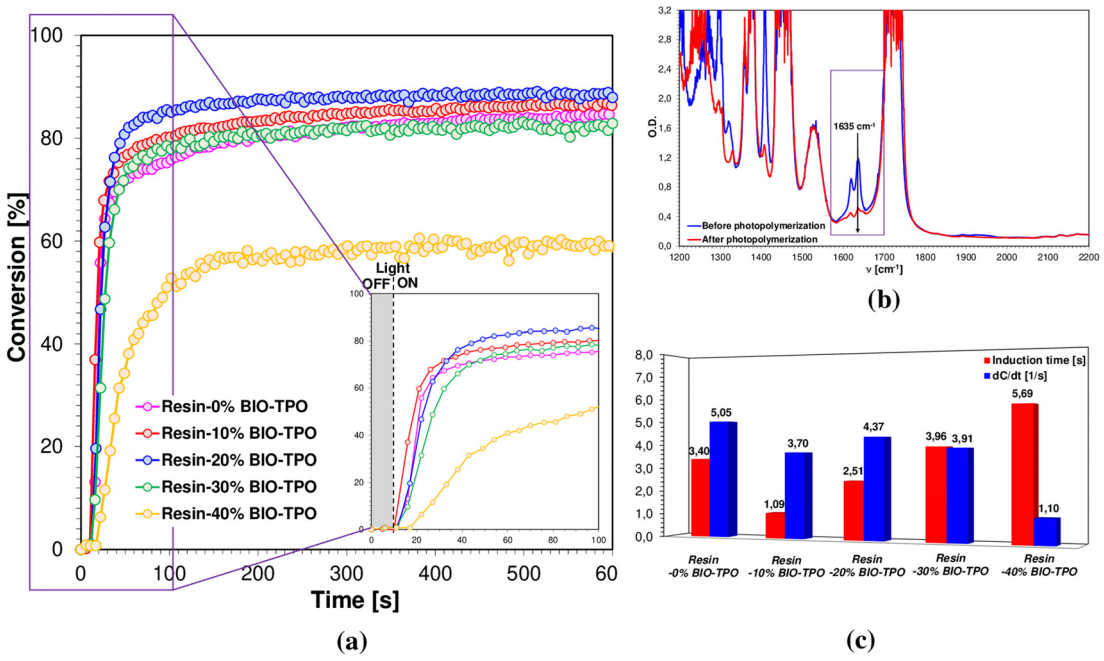

Fig. 5 Results achieved during radical photopolymerization of photocurable resins based on UDMA/HDDA monomers with different biobased monomer contents and the TPO initiator during VisLED@405 nm diode irradiation under atmospheric oxygen-limited conditions: (a) kinetic profiles representing the time dependence of functional group conversion, (b) FT-IR spectrum before and after the radical photopolymerization process, including the band characteristic of C=C bonds, and (c) diagram illustrating the values of the kinetic curve slope and induction time obtained during radical photopolymerization for resins with increasing amounts of the biobased monomer.

Table 3 The values of functional group conversion, kinetic curve slope, and induction time obtained from the radical photopolymerization kinetics of resins with various biobased monomer amounts

Resin	Conversion [%]	dC/dt [s^{-1}]	Induction time [s]
Resin-0% BIO-TPO	84	5.05	3.40
Resin-10% BIO-TPO	87	3.70	1.09
Resin-20% BIO-TPO	**88**	**4.37**	**2.51**
Resin-30% BIO-TPO	83	3.91	3.96
Resin-40% BIO-TPO	58	1.10	5.69

light incident on the studied sample was 5.58 mW cm^{-2}. The exact formulations of the resins are listed in Table 4.

Based on infrared spectroscopy measurements, it was found that addition of small amounts of amine synergists (1% or 2% by weight) did not affect the kinetics of the process, as the conversion of C=C bonds remained almost constant (88–89%) for both compositions with and without amine synergists. Addition of 5% amine synergist caused a significant deterioration of the kinetic parameters; it can be seen that the conversion of functional groups decreased (68%), and the value of the slope of the kinetic curve also declined, indicating that the process occurs more slowly (Fig. 6a and c). The functional group conversion was calculated based on the disappearance of the band characteristic of C=C bonds (Fig. 6b).

Table 5 summarizes the results obtained from radical photopolymerization carried out under atmospheric oxygen-limited conditions for resins with varying amounts of the amine synergist AS.

For comparison, analogous measurements were performed under aerobic conditions. We also investigated the effect of AS on this selected formulation under an oxygen atmosphere (Fig. 7a–c). A resin drop was placed on a pastille fabricated

Table 4 Formulation of photocurable resins polymerized by the radical mechanism based on the UDMA/HDDA/biobased monomer and the TPO initiator with the addition of the amine synergist AS

Resin	UDMA (w/w)	HDDA (w/w)	Biobased monomer (w/w)	Initiator (w/w)	Amine synergist
Resin-20% BIO-TPO	40%	40%	20%	1% TPO	0%
Resin-20% BIO-TPO-1%AS					1%
Resin-20% BIO-TPO-2%AS					2%
Resin-20% BIO-TPO-5%AS					5%

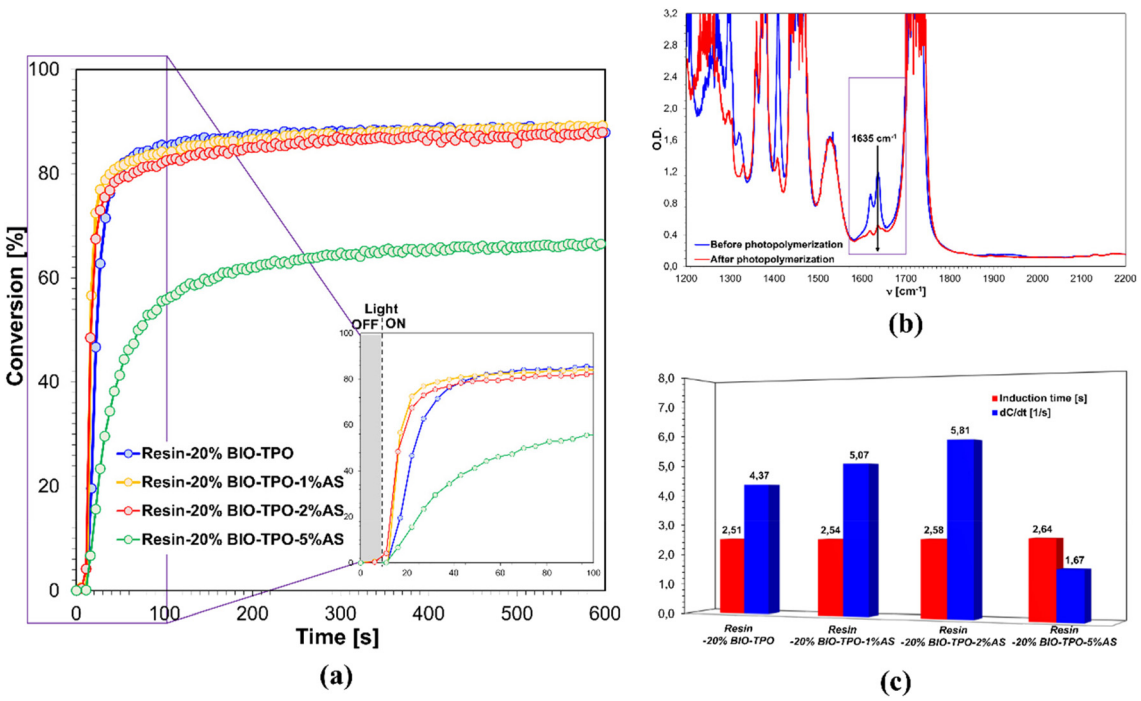

Fig. 6 Results achieved during radical photopolymerization of photocurable resins based on Resin-20%BIO-TPO with different amounts of the amine synergist AS during VisLED@405 nm diode irradiation under atmospheric oxygen-limited conditions: (a) kinetic profiles representing the time dependence of functional group conversion, (b) FT-IR spectrum before and after the radical photopolymerization process, including the band characteristic of C=C bonds, and (c) diagram illustrating the values of the kinetic curve slope and induction time obtained during radical photopolymerization for resins with increasing amounts of the amine synergist AS.

Table 5 The values of functional group conversion, kinetic curve slope, and induction time obtained from the radical photopolymerization kinetics of photocurable resins based on Resin-20%BIO-TPO with different amounts of the amine synergist AS under atmospheric oxygen-limited conditions

Resin	Conversion [%]	dC/dt [s^{-1}]	Induction time [s]
Resin-20% BIO-TPO	88	4.37	2.51
Resin-20% BIO-TPO-1%AS	89	5.07	2.54
Resin-20% BIO-TPO-2%AS	88	5.81	2.58
Resin-20% BIO-TPO-5%AS	67	1.67	2.64

Table 6 The values of functional group conversion, kinetic curve slope, and induction time obtained from the radical photopolymerization kinetics of photocurable resins based on Resin-20%BIO-TPO with different amounts of the amine synergist AS under aerobic conditions

Resin	Conversion [%]	dC/dt [s^{-1}]	Induction time [s]
Resin-20% BIO-TPO	0	—	—
Resin-20% BIO-TPO-1%AS	4	1.15	2.12
Resin-20% BIO-TPO-2%AS	12	1.21	2.08
Resin-20% BIO-TPO-5%AS	19	1.31	1.94

from barium fluoride. These results clearly demonstrate that the addition of the newly synthesized AS was effective under aerobic conditions. Although the conversion was 0% in the absence of AS, it increased to 19% when the AS concentration was 5%, as shown in Table 6. With an increase in the AS content in the investigated composition, a decrease in the oxygen inhibition effect was observed, which is a characteristic of radical photopolymerization. The higher the amount of the amine synergist AS in the photocurable resin, the higher the acrylate monomer conversion. For Resin-20% BIO-TPO, the degree of double-bond over-reactivity was 0%, confirming the absence of radical photopolymerization in the presence of atmospheric oxygen. With the increase in the AS compound in the photocurable compositions, the occurrence of radical photopolymerization and the reduction of the oxygen inhibition phenomenon can be observed. In the case of Resin-20% BIO-TPO-5%AS, in which the addition of the AS compound was 5% by weight, the conversion of C=C bonds was 19%. Reduced oxygen inhibition was caused by the presence of a tertiary amine and free thiol groups in the structure of the newly synthesized amine synergist.

Table 6 summarizes the results obtained from radical photopolymerization carried out under atmospheric oxygen conditions for resins with varying amounts of the amine synergist AS.

Moreover, for the AS compound and all the photocurable resins with the AS additive, thermal stability tests were carried out to verify how the AS additive affects the stability of the compositions and whether the established storage conditions

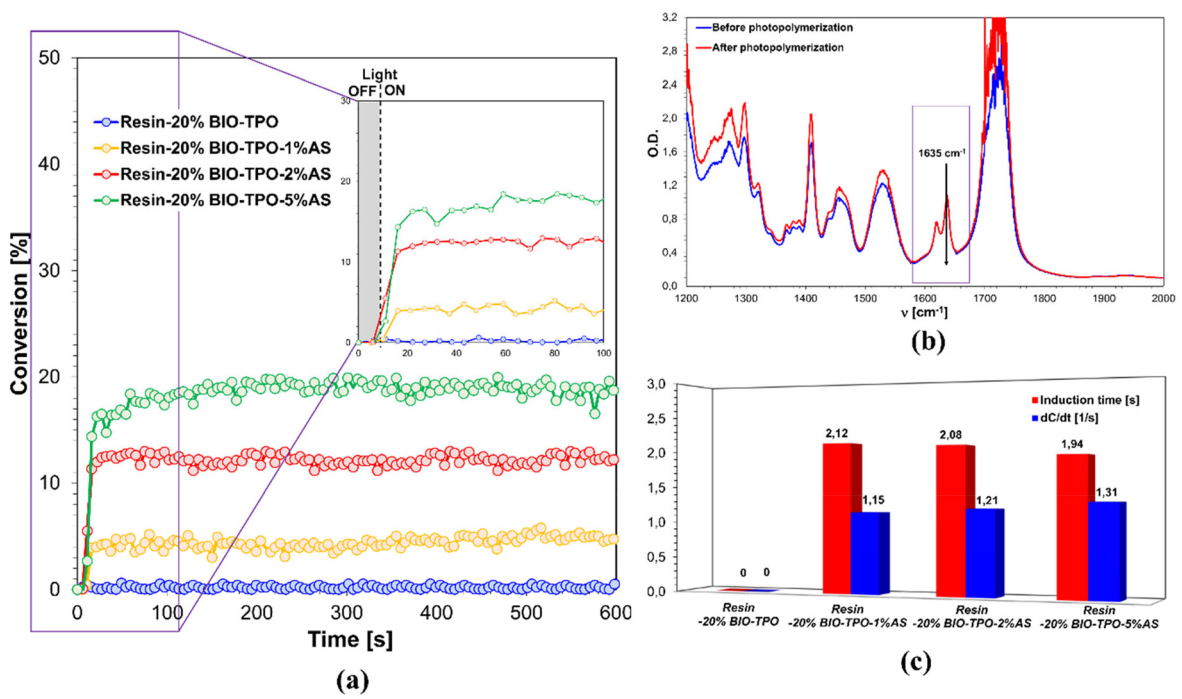

Fig. 7 Results achieved during radical photopolymerization of photocurable resins based on Resin-20%BIO-TPO with different amounts of the amine synergist AS during VisLED@405 nm diode irradiation under atmospheric oxygen conditions: (a) kinetic profiles representing the time dependence of functional groups' degree of conversion, (b) FT-IR spectrum before and after the radical photopolymerization process, including the band characteristic of C=C bonds, and (c) diagram illustrating the values of the kinetic curve slope and induction time obtained during radical photopolymerization for resins with increasing amounts of the amine synergist AS.

of the photocurable resins are necessary. The same temperature range was established for both the AS compound and AS-added resins. The test samples were heated in the range from 20 °C to 200 °C. The temperature measurement of the amine synergist carried out proved that the tested compound is stable over the entire range of temperatures investigated. Furthermore, at temperatures up to 200 °C, no significant thermal effects were observed for the photocurable resins without the AS additive (Resin-20% BIO-TPO) and with 1% (Resin-20% BIO-TPO-1%AS) and 2% AS (Resin-20% BIO-TPO-2%AS) additive. Therefore, at increased temperatures, the addition of AS and, consequently, thiol groups does not affect the thermal stability of the compositions. In the case of the addition of 5% AS to the photocurable resin (Resin-20% BIO-TPO-5%AS), thermal effects can be observed on the DSC plot, which appear at a temperature of about 140 °C, which, however, does not cause any problems related to the storage of resins at room temperature. No signs of instability of the examined formulations were observed during the tests. Time and temperature dependence graphs obtained by the DSC method for the AS compound and the resins in Table 4 are included in the SI (Fig. S11–S15).

3.3. 3D printing experiments with photocurable radical resins based on monomers: UDMA/HDDA/biobased monomer

Subsequently, based on kinetic studies, resins were selected for projector light-initiated 3D printing experiments. Three photocurable resins with a TPO photoinitiator were selected for 3D printing experiments. The first and most fundamental component was a resin containing a UDMA/HDDA/biobased monomer (Resin-20% BIO-TPO). Subsequently, the basic resin was modified to obtain further photocurable resins for visible-light-initiated additive processes. The first modification was the addition of 5% by weight of the amine synergist to Resin-20% BIO-TPO, resulting in Resin-20% BIO-TPO-5%AS. Next, the resin with 5% AS was further modified with 2% nanosilica addition (Resin-20% BIO-TPO-5%AS-2% SiO_2). The nanosilica was weighed in relation to the monomer matrix. The compositions were selected for the formation of spatial structures using light, as shown in Table 7.

Viscosity measurements of the monomer matrices were performed before the DLP 3D printing experiments were conducted. Viscosity is an extremely important parameter that determines the suitability of photocurable resins for light-initiated 3D printing. Low-viscosity resins are generally advantageous for the printing process; however, parts produced from such resins tend to exhibit high brittleness. Conversely, higher viscosity photocurable resins facilitate the fabrication of objects with improved mechanical properties. The viscosity value provides essential information about the 3D printing process, including considerations such as the need for support structures Table 8 presents the matrices subjected to viscosity measurements.

Table 8 Radical monomer matrices based on the UDMA/HDDA/biobased monomer differentiated by the amount of the amine synergist and nanosilica dedicated to viscosity measurements

Resin	UDMA (w/w)	HDDA (w/w)	Biobased monomer (w/w)	AS (w/w)	SiO_2 (w/w)
Matrix-20% BIO	40%	40%	20%	0%	0%
Matrix-20% BIO-5%AS				5%	0%
Matrix-20% BIO-5% AS-2% SiO_2				5%	2%

Viscosity measurements showed that the viscosity of Matrix-20% BIO containing UDMA/HDDA/biobased monomer was 728 mPa s. Addition of 5% AS to Matrix-20% BIO caused a slight increase in viscosity, and the viscosity of Matrix-20% BIO-5%AS became 740 mPa s. The viscosity of the matrix containing Matrix-20% BIO-5%AS-2% SiO_2 nanosilica is 850 mPa s. The viscosity experiments demonstrated that the investigated resins are high viscosity resins and show suitability for DLP 3D printing experiments. Fig. 8 presents the viscosity values of the monomer matrices utilized for projector-light-initiated 3D printing.

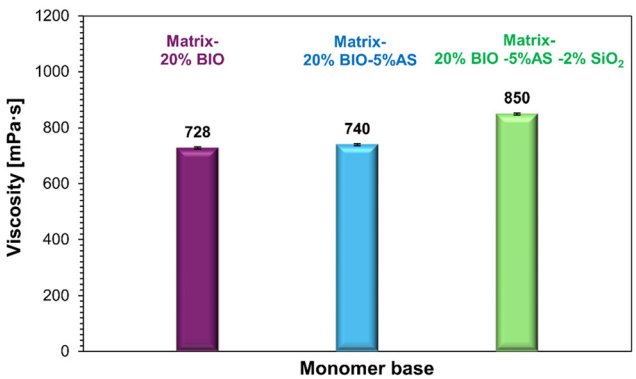

Fig. 8 Viscosity of radical monomer matrices based on UDMA/HDDA/biobased monomer differentiated by the amount of the amine synergist and nanosilica utilized for DLP 3D printing.

Table 7 Formulation of photocurable resins polymerized by the radical mechanism selected for 3D printing experiments based on the UDMA/HDDA/biobased monomer and the TPO initiator with different amounts of the amine synergist and nanosilica

Resin	UDMA (w/w)	HDDA (w/w)	Biobased monomer (w/w)	Initiator (w/w)	AS (w/w)	SiO_2 (w/w)
Resin-20% BIO-TPO	40%	40%	20%	1% TPO	0%	0%
Resin-20% BIO-TPO-5%AS					5%	0%
Resin-20% BIO-TPO-5%AS-2% SiO_2					5%	2%

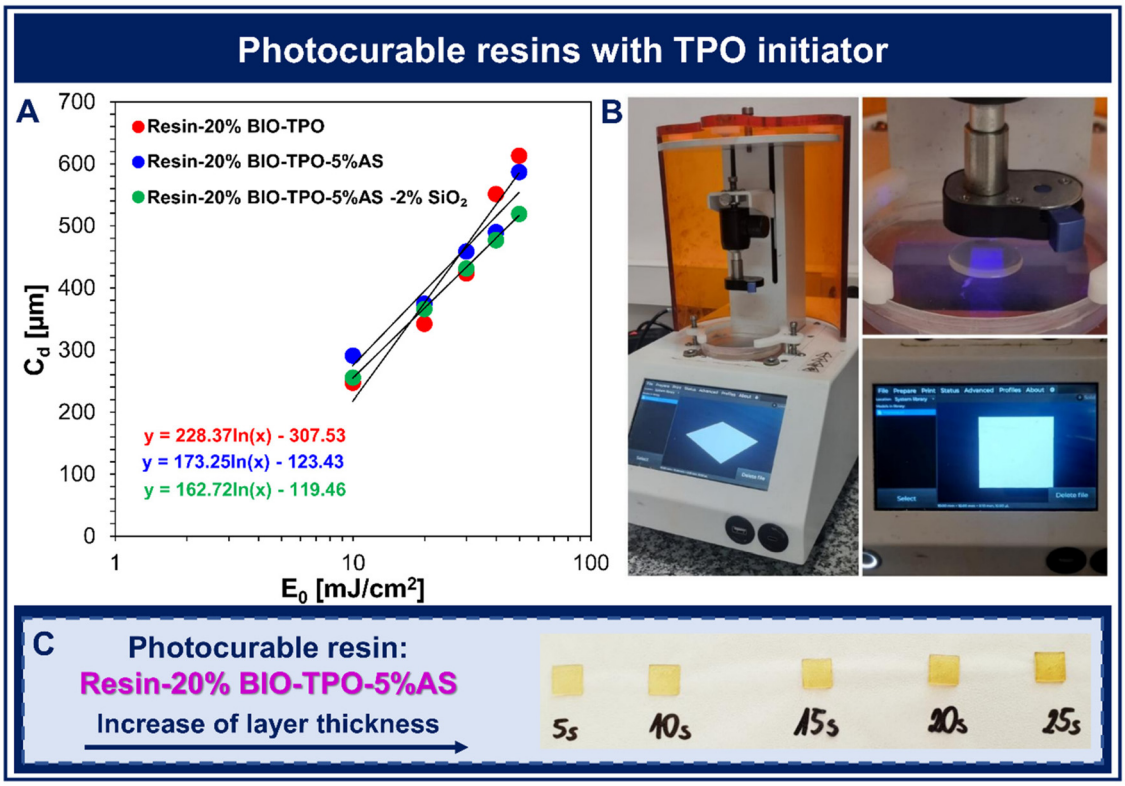

Fig. 9 Determination of fundamental parameters of 3D printing: (A) figure of basic Jacob's basic working curves determined for photocurable resins based on UDMA/HDDA/biobased monomer differentiated by the amount of the amine synergist and nanosilica; (B) the Lumen X+™ printer working with DLP technology during resin exposure to create a slice dedicated to determining the basic parameters of 3D printing; and (C) slices obtained from photocurable resins polymerizing according to the radical mechanism Resin-20% BIO-TPO-5%AS –2% SiO_2 received during exposure without the application of a printing platform using different exposure times.

Jacob's working curve test, an essential tool for determining the basic parameters of 3D printing, was performed. The test allowed the determination of the critical energy E_c and depth of light penetration D_p. The intersection of the obtained curves with the *X*-axis indicates the values of the critical energy, which indicates the minimum exposure required to cure the solid layer, whereas the slope of the curves indicates the depth of penetration (Fig. 9a). The test was based on printing five slices (1 × 1 cm) of each resin without a printing platform (Fig. 9b) using different resin exposure times (5, 10, 15, 20, and 25 s – Fig. 9c). Based on the thickness of the slices measured with a micrometer screw, exposure time of a slice, and intensity of light incident on the printing object during printing, the basic printing parameters defining the effectiveness of the photopolymerizing resin were determined. Based on the quotient of the curing time of each slice and the intensity of the light incident on the printed slice (measured with a ThorLabs PM 160 Optical Power Meter), E_0 (light energy at the surface [mJ cm^{-2}]) was calculated.

When compared, it can be seen that the addition of AS decreased the E_c value to 2.04 mJ cm^{-2} (Resin-20% BIO-TPO-5%AS) from 3.84 mJ cm^{-2} (Resin-20% BIO-TPO). The decrease in critical energy implies that less energy is required for curing. Moreover, it can be seen that the penetration depth also decreased when AS was incorporated. The decreased light penetration depth indicates greater control over the resolution and quality of the printing. Thus, it can be said that the synthesized AS is an intriguing additive for 3D printing applications. When fillers are used in 3D printing resins, more energy is required for curing and E_c increases. We added 2% SiO_2 nanoparticles to 5% AS-containing formulations and found that the E_c was almost the same as that of the filler-free formulation. This situation was attributed to the oxygen inhibition function of AS, which increased the curing speed and decreased E_c. Table 9 summarizes the 3D printing parameters obtained during Jacob's working curve test.

Table 9 Fundamental printing parameters determined by Jacob's working curve method for photocurable resins based on the UDMA/HDDA/biobased monomer differentiated by the amount of the amine synergist and nanosilica with the TPO initiator

Resin	Equation	Critical energy [mJ cm^{-2}]	Light penetration depth [µm]
Resin-20% BIO-TPO	$y = 228.37\ln(x) - 307.53$	3.84	216.96
Resin-20% BIO-TPO-5%AS	$y = 173.25\ln(x) - 123.43$	2.04	166.94
Resin-20% BIO-TPO-5%AS -2% SiO_2	$y = 162.72\ln(x) - 119.46$	2.08	162.08

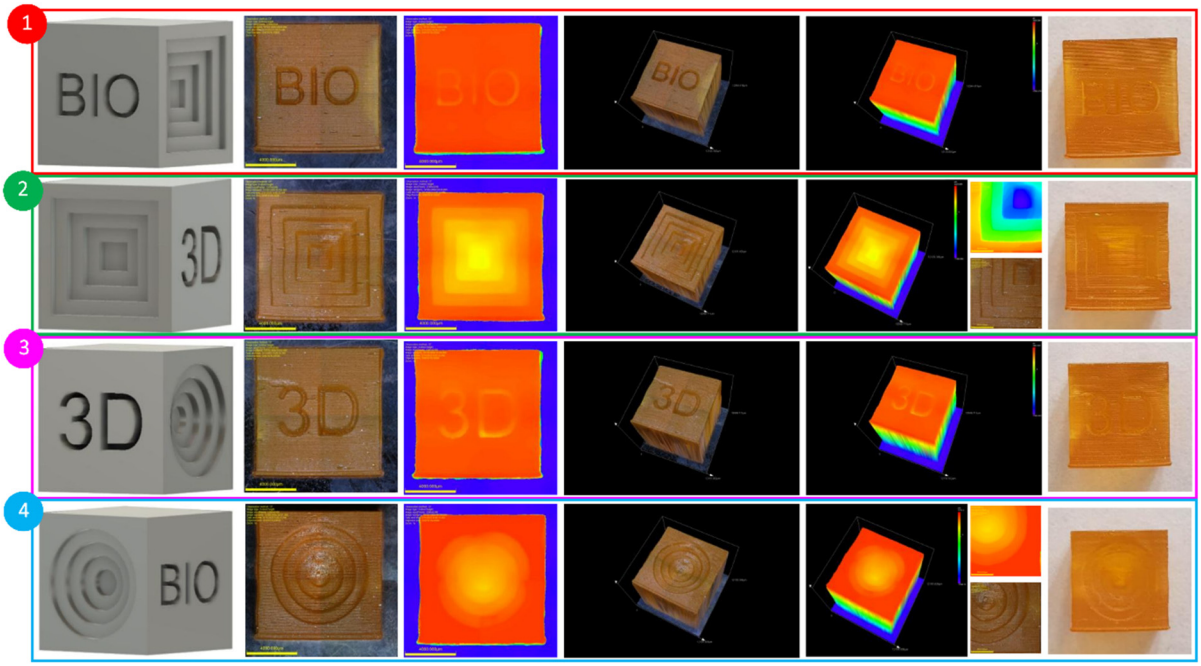

Fig. 10 Graphics showing the 3D model, 2D images and 3D images of prints obtained with Resin-20% BIO-TPO-5%AS-2% SiO_2.

The very promising results obtained during Jacob's working curve test allowed the resins to be applied in the printing of three-dimensional structures. The same printer settings were used for all the resins. The power of the printing device was 20%, which provides a light intensity incident on the printing object of 1.99 mW cm^{-2}. The exposure time for the initial printed layers was 30 s, while that for the remaining layers was 8 s. The thickness of each layer is 100 μm. The obtained structures were visualized on an optical microscope, as well as on a scanning electron microscope. The following graph illustrates the object obtained from Resin-20% BIO-TPO-5%AS-2% SiO_2 (Fig. 10). Graphics of the prints obtained with the other resins (Resin-20% BIO-TPO and Resin-20% BIO-TPO-5%AS) are shown in the SI (Fig. S16–S17a).

In addition, SEM imaging was performed on Resin-20% BIO-TPO-5%AS and Resin-20% BIO-TPO-5%AS-2% SiO_2 prints to study the resolution of the obtained 3D structures. Visualization using scanning electron microscopy (SEM) enabled the acquisition of precise images of the surface, which provided information about the high quality of the layers of the resulting print. Fig. 11 shows the graph obtained for the structure printed with Resin-20% BIO-TPO-5%AS-2% SiO_2. A graphic of a 3D object printed with Resin-20% BIO-TPO-5%AS is shown in the SI (Fig. S17b).

SEM analysis of the print obtained from the photocurable resin Resin-20% BIO-TPO-5%AS-2% SiO_2 showed that the resulting print has a high resolution, as evidenced by the clearly visible layers. Additionally, based on the above-mentioned SEM analysis, it can also be deduced that Resin-20% BIO-TPO-5%AS-2% SiO_2 is highly suitable for DLP 3D printing, as the thickness of the obtained layers is very similar to the model layer thickness of 100 μm, confirming that the investigated resin is characterized by very low polymerization shrinkage.

3.4. The application of AS as a co-initiator for cationic photoinitiators to initiate radical photopolymerization

The first stage of this research investigated the effects of different AS contents on the kinetics of the photopolymerization process and DLP 3D printing. The second stage of the research is related to the application of AS in two-component initiator systems, where commercial cationic photoinitiators based on iodonium salts (IOD and HIP), characterized by an absorption spectrum reaching up to approximately 320 nm, were applied as photoinitiators. The use of amines in two-component initiator systems allows for the generation of reactive radicals that can initiate the radical photopolymerization process using a light source with a wavelength that commercial iodonium salts cannot absorb. Infrared spectroscopy was used to compare the amine synergist AS with EDB as co-initiators for initiating radical photopolymerization. For this purpose, four resins differentiated by the initiator system were prepared. The resin compositions are listed in Table 10. The compositions were prepared to contain twice the molar excess of amine relative to the iodonium salt.

Radical photopolymerization was performed under conditions of limited access to atmospheric oxygen, and a UV-LED diode emitting radiation with a wavelength of λ = 340 nm was applied as the light source. The light source was turned on 10 s after the measurement. The light intensity incident on the photopolymerizing radical resin is 6.99 mW cm^{-2}. Fig. 12 illus-

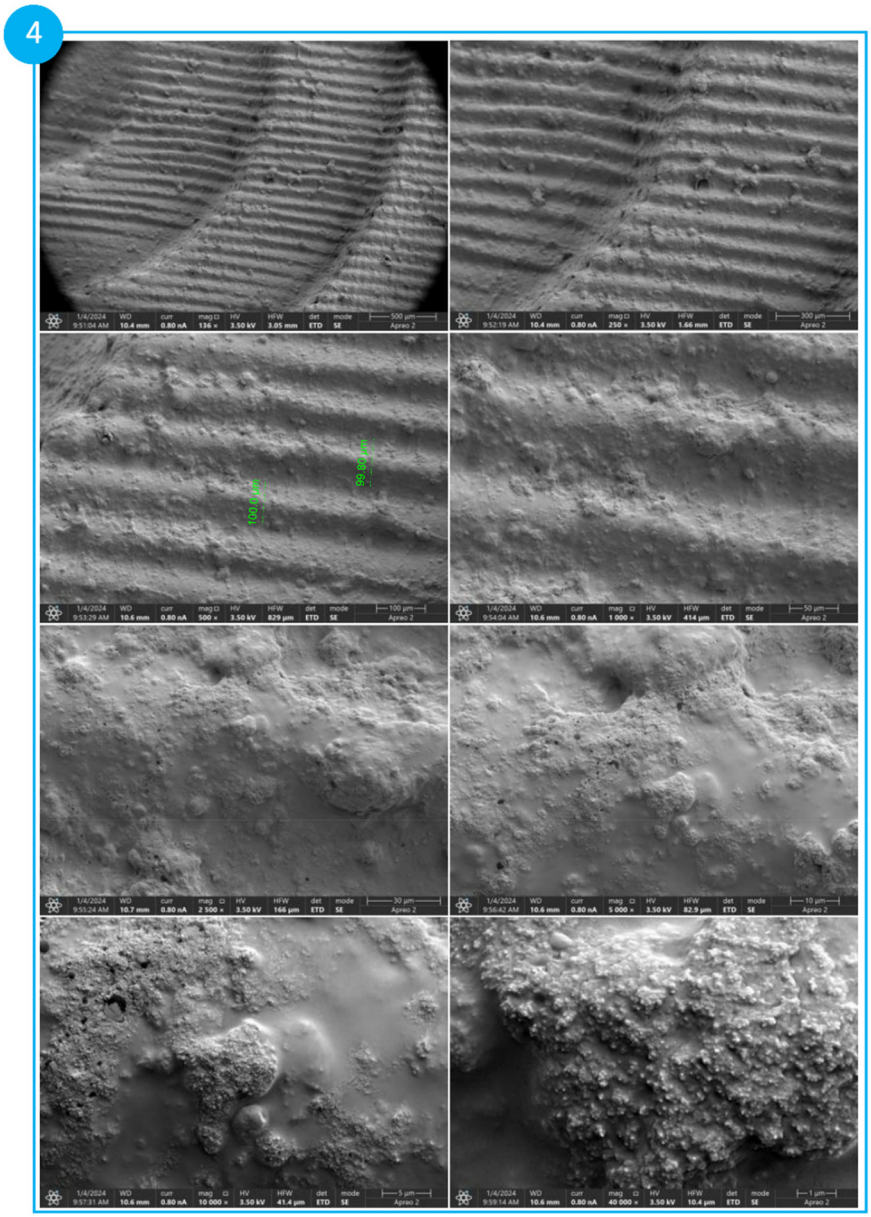

Fig. 11 SEM images of a print obtained with Resin-20% BIO-TPO-5%AS-2% SiO_2 employing DLP technology.

Table 10 Resins polymerizing according to the radical mechanism using a two-component initiator system based on commercial cationic photoinitiators based on iodonium salts (IOD or HIP) and amine co-initiators (AS or EDB)

Resin	Monomer	AS [mol]	IOD [mol]	EDB [mol]	HIP [mol]
Resin-AS+IOD_TMPTA	TMPTA	4.18×10^{-5}	2.09×10^{-5}	—	—
Resin-EDB+IOD_TMPTA		—	2.09×10^{-5}	4.18×10^{-5}	—
Resin-AS+HIP_TMPTA		4.18×10^{-5}	—	—	2.09×10^{-5}
Resin-EDB+HIP_TMPTA		—	—	4.18×10^{-5}	2.09×10^{-5}

trates the results obtained during the radical photopolymerization of the TMPTA monomer and the spectra before and after photopolymerization, indicating the band characteristics of acrylates.

As shown in Fig. 12, two-component initiator systems with AS were more effective than those containing EDB. The TMPTA acrylate monomer conversion was approximately 50% for resins containing AS + IOD (Resin-AS+IOD_TMPTA) and

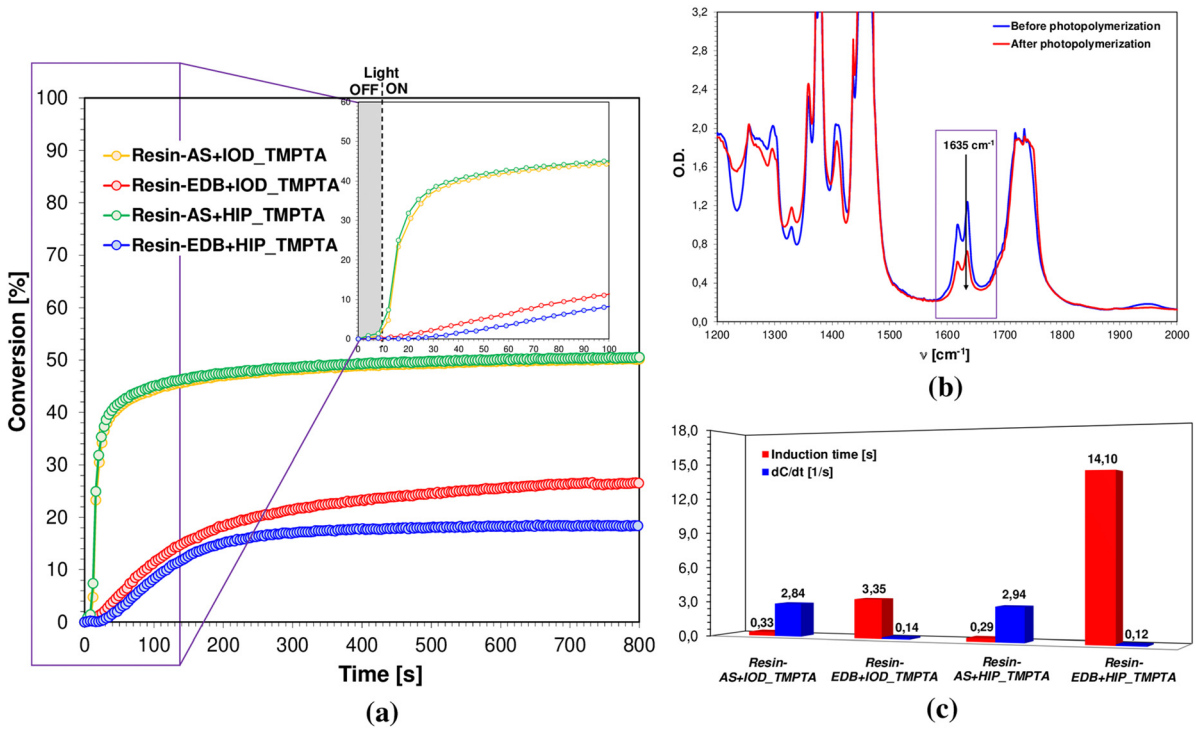

Fig. 12 Results achieved during radical photopolymerization of photocurable resins based on the TMPTA monomer containing a two-component initiator system based on commercial cationic photoinitiators based on iodonium salts (IOD or HIP) and amine co-initiators (AS or EDB) during UV-LED@340 nm diode irradiation under atmospheric oxygen-limited conditions: (a) kinetic profiles representing the time dependence of acrylate groups' degree of conversion, (b) FT-IR spectrum before and after the radical photopolymerization process, including the band characteristic of acrylate groups, and (c) diagram illustrating the values of the kinetic curve slope and induction time obtained during radical photopolymerization for resins with different two-component initiator systems.

Table 11 The values of acrylate conversion, kinetic curve slope and induction time obtained from the radical photopolymerization kinetics of resins containing a two-component initiator system based on commercial cationic photoinitiators based on iodonium salts (IOD or HIP) and amine co-initiators (AS or EDB)

Resin	Conversion [%]	dC/dt [s^{-1}]	Induction time [s]
Resin-AS+IOD_TMPTA	50	2.84	0.33
Resin-EDB+IOD_TMPTA	27	0.14	3.35
Resin-AS+HIP_TMPTA	51	2.94	0.29
Resin-EDB+HIP_TMPTA	18	0.12	14.10

Table 12 Resins polymerizing according to the radical mechanism containing a two-component initiator system based on commercial cationic photoinitiators based on the iodonium salt 7MP and the amine co-initiator AS

Resin	7MP [mol]	AS [mol]	Monomer
Resin-7MP : AS_1 : 0	4.18×10^{-5}	—	TMPTA
Resin-7MP : AS_1 : 1		4.18×10^{-5}	
Resin-7MP : AS_1 : 2		8.36×10^{-5}	
Resin-7MP : AS_1 : 3		1.25×10^{-4}	
Resin-7MP : AS_1 : 4		1.67×10^{-4}	
Resin-7MP : AS_1 : 5		2.09×10^{-4}	

AS+HIP (Resin-AS+HIP_TMPTA), whereas analogous resins with EDB only reacted at 18% (Resin-EDB+HIP_TMPTA) and 27% (Resin-EDB+IOD_TMPTA), as shown in Table 11. Based on preliminary application studies, the newly synthesized amine synergist AS has a significant advantage over commercially available EDB. The better results obtained for AS than for EDB are due to differences in the molar values of the extinction coefficients, as well as the oxidation potential. The molar extinction coefficient for EDB reached very low values at λ = 340 nm, whereas the oxidation potential of EDB was higher than that of the newly synthesized amine synergist AS.

The next stage was to prepare a radical resin with a two-component initiator system containing the amine synergist AS and commercial cationic photoinitiators based on the iodonium salt 7MP ((7-methoxy-4-methylcoumarin-3-yl)phenyliodonium hexafluorophosphate). The radical resin formulations used are listed in Table 12. Because the absorption range of the photoinitiator 7MP extends into the visible range, Vis-LED@405 nm was employed. The light intensity incident on the photopolymerizing radical resin is 15.98 mW cm^{-2}.

The investigation involved checking the effect of the addition of amine synergists on the initiation of radical photopolymerization, where a typical cationic photoinitiator was applied as the photoinitiator, which is ideal for initiating the cationic photopolymerization of epoxy and vinyl monomers, as shown in the literature.[63] As shown in Fig. 13, the cationic

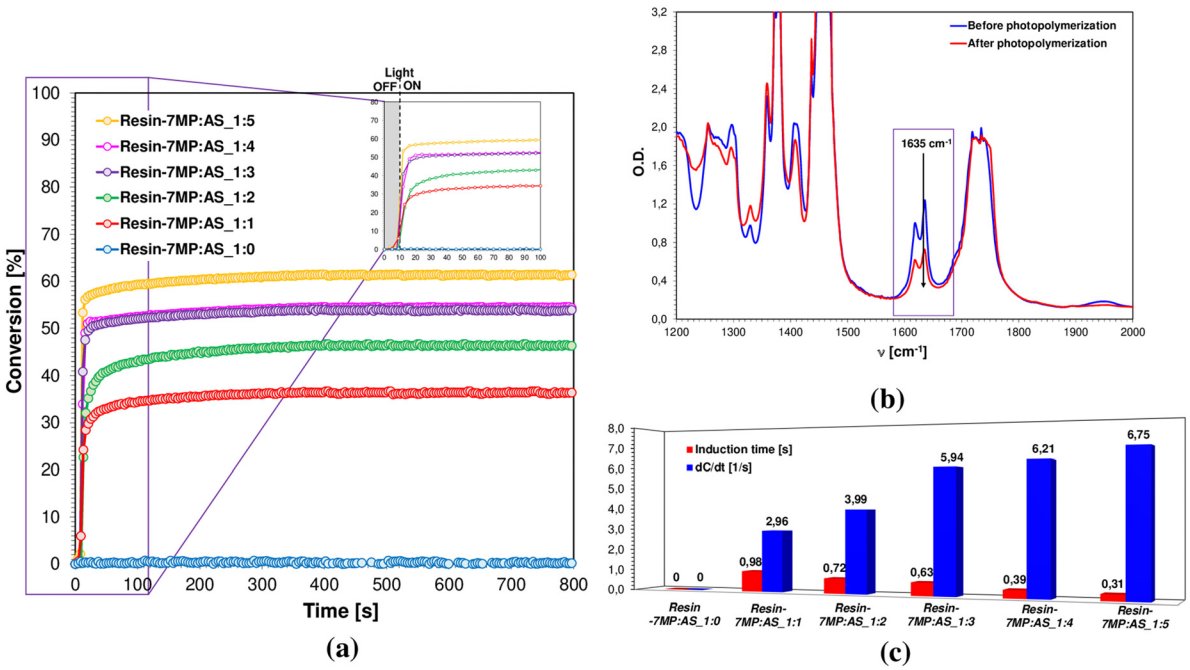

Fig. 13 Results achieved during radical photopolymerization of photocurable resins based on the TMPTA monomer containing a two-component initiator system based on a commercial cationic photoinitiator based on the iodonium salt 7MP and the amine co-initiator AS during Vis-LED@405 nm diode irradiation under atmospheric oxygen-limited conditions: (a) kinetic profiles representing the time dependence of acrylate groups' degree of conversion, (b) FT-IR spectrum before and after the radical photopolymerization process, including the band characteristic of C═C bonds, and (c) diagram illustrating the values of the kinetic curve slope and induction time obtained during radical photopolymerization of resins containing the 7MP initiator and varying amounts of the amine co-initiator AS.

initiator 7MP was not suitable for initiating radical photopolymerization of TMPTA, as the resulting conversion of acrylate groups was 0%. As the amount of the co-initiator AS in the composition increases, higher conversions of acrylate groups can be observed, reaching 61% at a fivefold molar excess of AS relative to the photoinitiator 7MP. The combination of AS with a cationic initiator allows the generation of reactive radicals, and consequently, the efficient initiation of radical photopolymerization under visible light. With the increasing amount of AS in the photocurable resins, it is possible to observe not only an increase in the degree of over-reactivity of the functional groups, but also an increase in the speed of the photopolymerization process, as evidenced by the increasing value of the slope of the kinetic curve and the decreasing value of the induction time (Fig. 13a and c). Fig. 13b presents the disappearance of the band characteristic of the acrylate groups during radical photopolymerization of the TMPTA monomer.

Table 13 summarizes the results obtained from radical photopolymerization carried out under atmospheric oxygen-limited conditions for resins containing the 7MP initiator by varying the amount of the co-initiator AS.

The final research stage on the application of a two-component initiator system with AS as the co-initiator and 7MP as the photoinitiator was the 3D printing experiment. An initiator system containing twofold molar excess of the amine relative to the 7MP initiator was chosen for the investigation. The two resins were polymerized according to a free radical mechanism. One contained UDMA/HDDA monomers (50/50 w/w) – Resin-7MP : AS (1 : 2)_UDMA/HDDA, whereas the other contained an additional biobased monomer UDMA/HDDA/biobased monomer (40/40/20 w/w) – Resin-7MP : AS (1 : 2)_UDMA/HDDA/BIO. First, kinetic studies were performed on the prepared compositions to determine the effect of biobased monomer addition on the kinetics of the radical photopolymerization process. The research was conducted by applying Fourier transform infrared spectroscopy, where an LED emitting radiation with a wavelength of λ = 405 nm was used as the light source. This allowed for the creation of conditions analogous to 3D printing, where the light source was a projector with the same wavelength.

Table 13 The values of acrylate conversion, kinetic curve slope and induction time obtained from the radical photopolymerization kinetics of resins containing the 7MP initiator and varying amounts of the amine co-initiator AS

Resin	Conversion [%]	dC/dt [s^{-1}]	Induction time [s]
Resin-7MP : AS_1 : 0	0	—	—
Resin-7MP : AS_1 : 1	36	2.96	0.98
Resin-7MP : AS_1 : 2	46	3.99	0.72
Resin-7MP : AS_1 : 3	53	5.94	0.63
Resin-7MP : AS_1 : 4	54	6.21	0.39
Resin-7MP : AS_1 : 5	61	6.75	0.31

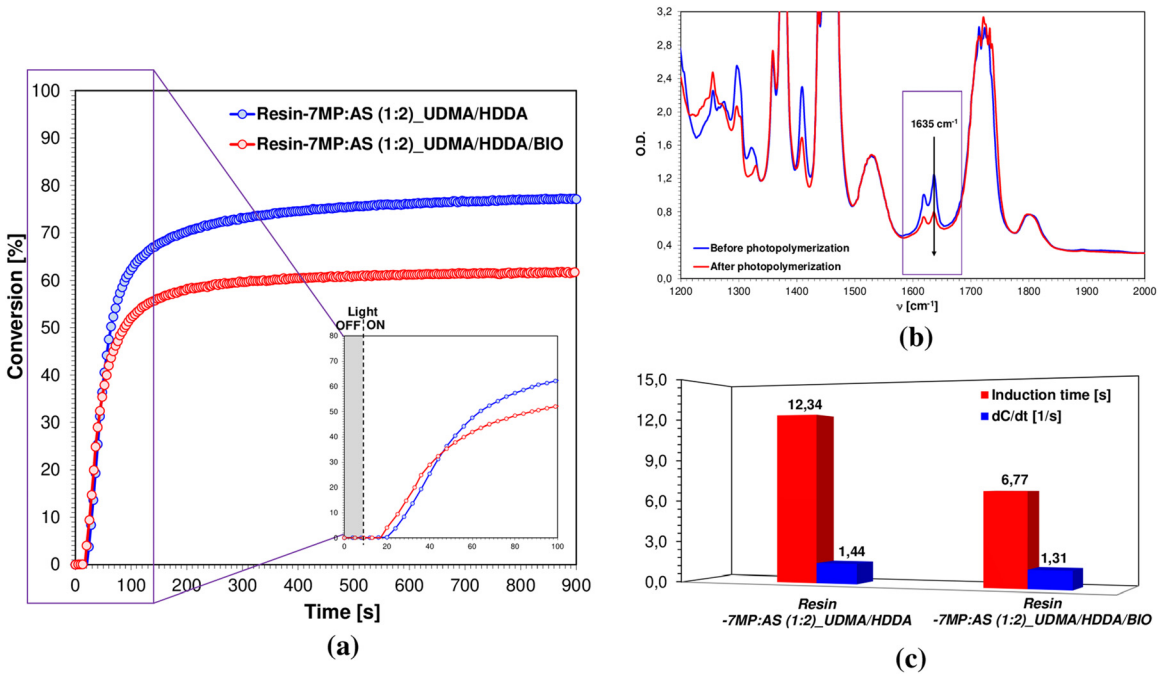

Fig. 14 Results achieved during radical photopolymerization of photocurable resins based on the UDMA/HDDA monomer containing a two-component initiator system based on a commercial cationic photoinitiator based on the iodonium salt 7MP and the amine co-initiator AS during Vis-LED@405 nm diode irradiation under atmospheric oxygen-limited conditions: (a) kinetic profiles representing the time dependence of functional groups' degree of conversion, (b) FT-IR spectrum before and after the radical photopolymerization process, including the band characteristic of C=C bonds, and (c) diagram illustrating the values of the kinetic curve slope and induction time obtained during radical photopolymerization of resins containing the 7MP initiator and varying amounts of the amine co-initiator AS.

As shown in Fig. 14, addition of 20% biobased monomer to the UDMA/HDDA mixture caused a decrease in the degree of functional group conversion, which was negligible at 15%. Despite obtaining a lower conversion for the resin with the addition of biobased monomers (Resin-7MP : AS (1 : 2)_UDMA/HDDA/BIO), the other kinetic parameters improved, the induction time decreased, and the value of the slope of the kinetic curve increased (Table 14).

The promising results obtained for radical resins with the AS + 7MP two-component initiation system allow them to be further developed and explored for potential applications in 3D printing. First, the viscosity properties of the resins dedicated to 3D printing were measured. Therefore, two formulations were prepared: radical monomers and amine synergists. The precise formulation for viscosity research is presented in Table 15.

Viscosity measurements showed that Matrix-UDMA/HDDA has a viscosity of 540 mPa s. Modification of the above-mentioned matrix by addition of 20% biobased monomer (Matrix-UDMA/HDDA/BIO) results in a significant increase in the viscosity of the resin formulation (738 mPa s), suggesting that the structures obtained from the photocurable resin with the addition of a biobased monomer will have better mechanical properties compared to the resin without the addition of a biobased monomer. Fig. 15 illustrates the viscosity values for the different monomer matrices.

For photocurable resins: Resin-7MP : AS (1 : 2)_UDMA/HDDA and Resin-7MP : AS (1 : 2)_UDMA/HDDA/BIO, Jacob's working curve test was carried out using the same procedure as for resins containing the TPO initiator (Table 16).

Jacob's working curve test showed that addition of 20% biobased monomer to the UDMA/HDDA mixture resulted in an

Table 14 The values of functional group conversion, kinetic curve slope, and induction time obtained from the radical photopolymerization kinetics of resins containing the 7MP + AS two-component initiating system employed in subsequent 3D printing experiments

Resin	Conversion [%]	dC/dt [s^{-1}]	Induction time [s]
Resin-7MP : AS (1 : 2)_UDMA/HDDA	77	1.44	12.34
Resin-7MP : AS (1 : 2)_UDMA/HDDA/BIO	62	1.31	6.77

Table 15 Radical monomer matrices based on UDMA/HDDA differentiated by the amount of the biobased monomer dedicated to viscosity measurements

Resin	UDMA (w/w)	HDDA (w/w)	Biobased monomer (w/w)	AS [mol]
Matrix-UDMA/HDDA	50	50	—	8.36×10^{-5}
Matrix-UDMA/HDDA/BIO	40	40	20	

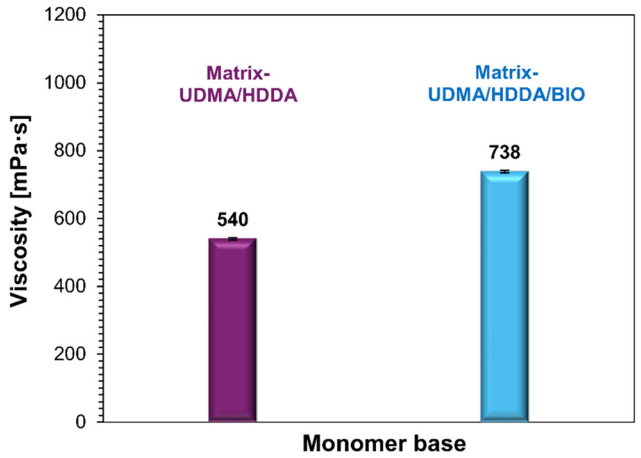

Fig. 15 Viscosity of radical monomer matrices based on UDMA/HDDA differentiated by the amount of the biobased monomer utilized for DLP 3D printing.

Table 16 Fundamental printing parameters determined by Jacob's working curve method for resins based on UDMA/HDDA differentiated by the amount of the biobased monomer with the 7MP initiator

Resin	Equation	Critical energy [mJ cm^{-2}]	Light penetration depth [μm]
Resin-7MP : AS (1 : 2) _UDMA/HDDA	$y = 162.12 \ln(x) - 281.79$	5.69	161.78
Resin-7MP : AS (1 : 2) _UDMA/HDDA/BIO	$y = 145.59 \ln(x) - 570.31$	50.26	141.38

almost nine-fold increase in the critical energy value while reducing the depth of light penetration, which is not beneficial for 3D printing. The exposure time for the initial layers of both Resin-7MP : AS (1 : 2)_UDMA/HDDA and Resin-7MP : AS (1 : 2) _UDMA/HDDA/BIO was 100 s, while that for the remaining layers was 30 s. The difference is in the intensity of the light incident on the printed object. For Resin-7MP : AS (1 : 2) _UDMA/HDDA, the light intensity during printing was 2.99 mW cm^{-2}, whereas that of Resin-7MP : AS (1 : 2)_UDMA/HDDA/BIO was 3.98 mW cm^{-2}. The thickness of the printed layer in both cases was 100 μm. The plots of the dependence of light penetration depth D_p on the critical energy E_c for each of the studied resins with the 7MP initiator are presented in the SI (Fig. S18). Fig. 16a presents images of Resin-7MP : AS (1 : 2)_UDMA/HDDA printed on an optical microscope, whereas Fig. 16b illustrates images of this print taken on a scanning electron microscope. The SEM image confirmed the high quality of the obtained three-dimensional object. Single layers can be seen, as well as pixels, which indicates that the 7MP + AS two-component initiator system is highly suitable for initiating radical photopolymerization and can successfully find applications in light-initiated 3D printing. In addition, as shown in Fig. 16b, the pixels of the printed object are approximately 50 μm in size, which is equal to the resolution of the printer employed, indicating very low polymerization shrinkage.

Moreover, microscopic analysis of the object printed from Resin-7MP : AS (1 : 2)_UDMA/HDDA/BIO was performed. According to Fig. 17, the printed shapes are visible, but defects between the printed layers can also be seen. Based on the obtained prints, it can be concluded that the addition of a biomonomer results in the deterioration of print quality, but is a very promising approach for biomedical applications. The SEM analysis of the print obtained from Resin-7MP : AS (1 : 2)_UDMA/HDDA/BIO is presented in the SI (Fig. S19).

In addition, hardness tests were conducted on the prints received from Resin-7MP : AS (1 : 2)_UDMA/HDDA and Resin-7MP : AS (1 : 2)_UDMA/HDDA/BIO using the Shore scale. The printout obtained from Resin-7MP : AS (1 : 2)_UDMA/HDDA was characterized by a hardness of 71 ± 1, whereas the printout obtained from Resin-7MP : AS (1 : 2)_UDMA/HDDA/BIO with the addition of biobased monomers was characterized by a hardness of 83 ± 2. The high viscosity of the biobased monomer increased the viscosity of the UDMA/HDDA monomer matrix, resulting in improved mechanical properties. Summarizing the validity of the application of the biobased monomer to the photopolymerization process, it can be concluded that the addition of the biobased monomer reduces the induction time during the radical photopolymerization process, which is suitable for projector light-initiated 3D printing, and improves the mechanical properties of the printed three-dimensional structures.

3.4.1. Physical, optical, thermal, and surface wettability properties of the selected compositions. We investigated the effect of the amine synergist on the optical and thermal properties of three selected compositions. The first composition (Control) was composed of 40% UDMA, 40% HDDA, 20% biobased monomer, and 1% TPO. The second selected composition was the same as the first (control), except that it contained an additional 5% AS. The second formulation was named ControlAS. Finally, a third formulation (ControlSiNP) was prepared by adding 2% SiO_2 nanoparticles to ControlAS. First, we determined the gel content of the photosets *via* Soxhlet extraction with acetone. As shown in Fig. 18a, the gel content of the control was 96%, which decreased with the addition of the amine synergist. The addition of silica nanoparticles led to a further decrease in the gel content. Nevertheless, the gel content of the photosets was acceptable. Although the addition of AS led to a decline in the double-bond conversion owing to its light absorption and decreasing cure depth, a significant improvement was observed in the surface wettability properties (Fig. 18b). The water contact angle of the control formulation was 40° ± 3. This value was attributed to the presence of polar urethane bonds (UDMA), polar imine bonds, and oxygen inhibition, which led to the polar surface features. The addition of the amine synergist increased the contact angle to 63° ± 2°, which can be ascribed to decreased oxygen inhibition. The addition of silica nanoparticles did not lead to a significant change in the contact

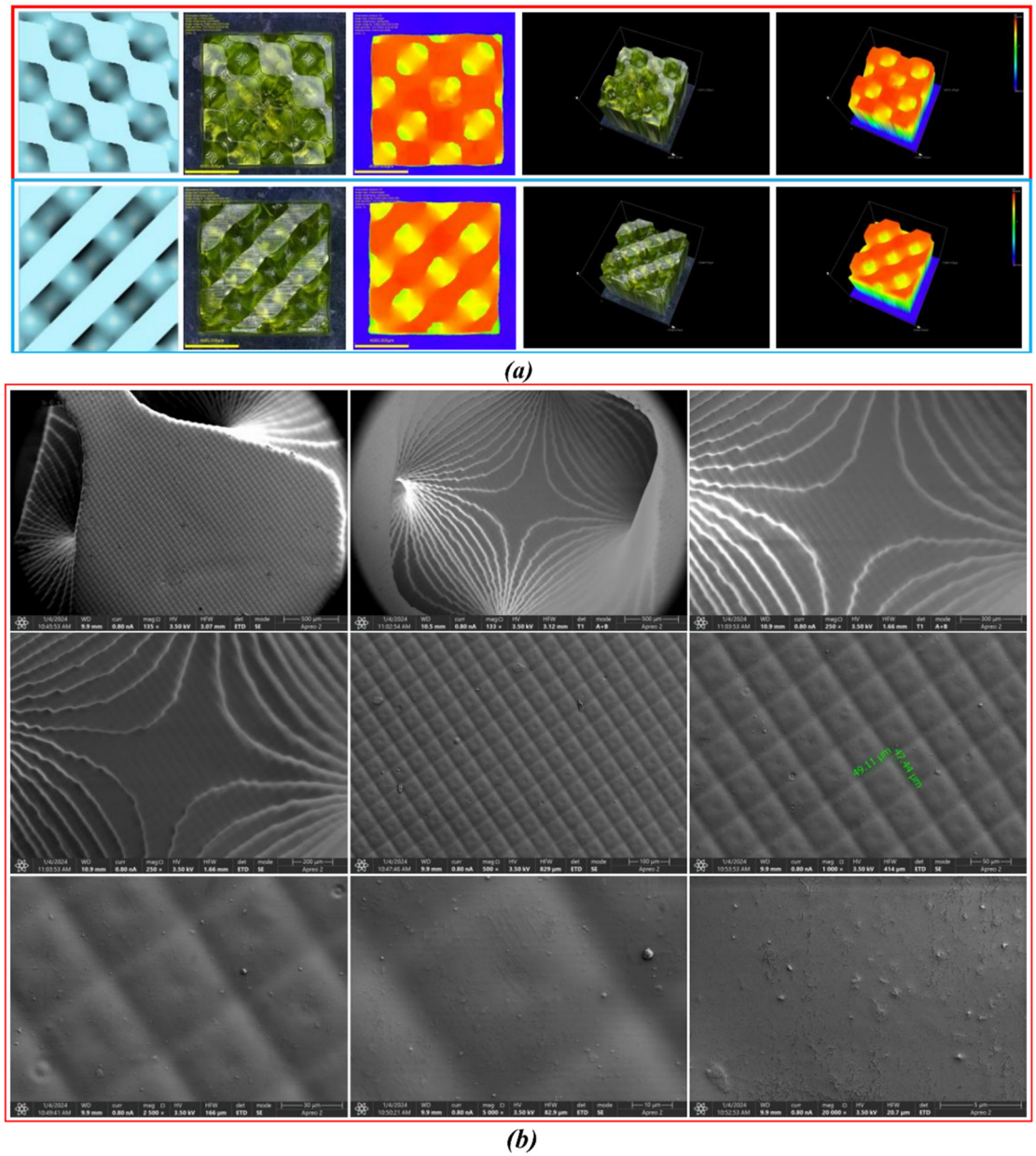

Fig. 16 Graphics showing the 3D model, 2D images and 3D images of prints obtained with Resin-7MP : AS (1 : 2)_UDMA/HDDA: (a) optical microscopy analysis and (b) SEM analysis.

angle values, owing to the relatively low amount within the composition.

The prepared photosets were yellow because of the presence of the vegetable-oil-based DVDMA. We assessed the optical properties of the photosets by recording their light transmission spectra (Fig. 18c). As observed from these spectra, the control formulation displayed a higher level of light transmission in the 400–800 nm region. The addition of AS led to a decline in the light transmission percentage owing to the light absorption of AS. The addition of silica nanoparticles also decreased the penetration of light owing to the light scattering and blocking effect of the nanoparticles.

Finally, the thermal properties of the photosets were investigated. TGA thermograms of the photosets are shown in Fig. 18d. All samples displayed similar degradation profiles. All studied compositions exhibited weight losses between 30 and 300 °C which were attributed to the decomposition of the unreacted monomers and photoinitiator residues. The amine synergist-containing samples (ControlAS and ControlSiNP) displayed relatively higher weight losses in this region (30–300 °C) than the Control formulation. This finding is in good agreement with the gel content values. The maximum weight loss temperature for all the compositions was approximately 450 °C, and no significant difference was found among the

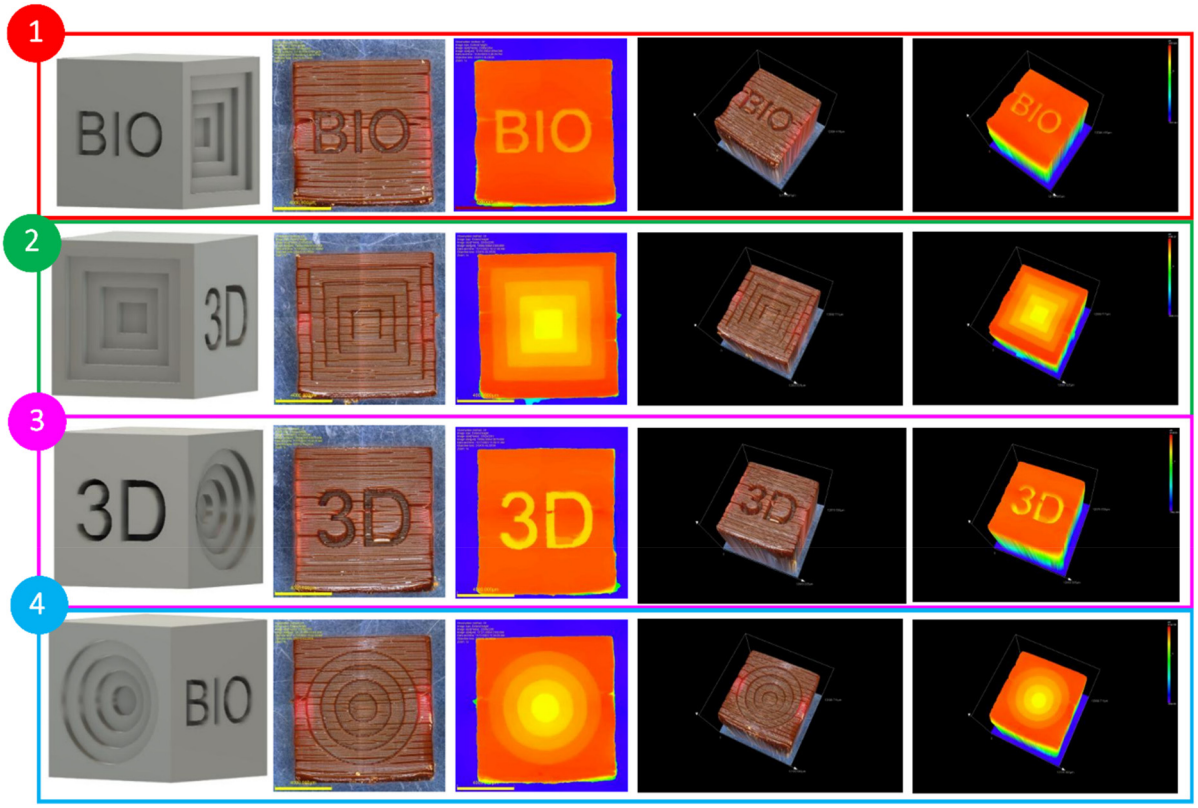

Fig. 17 Graphics showing the 3D model, 2D images and 3D images of prints obtained with Resin-7MP : AS (1 : 2)_UDMA/HDDA/BIO employing optical microscopy.

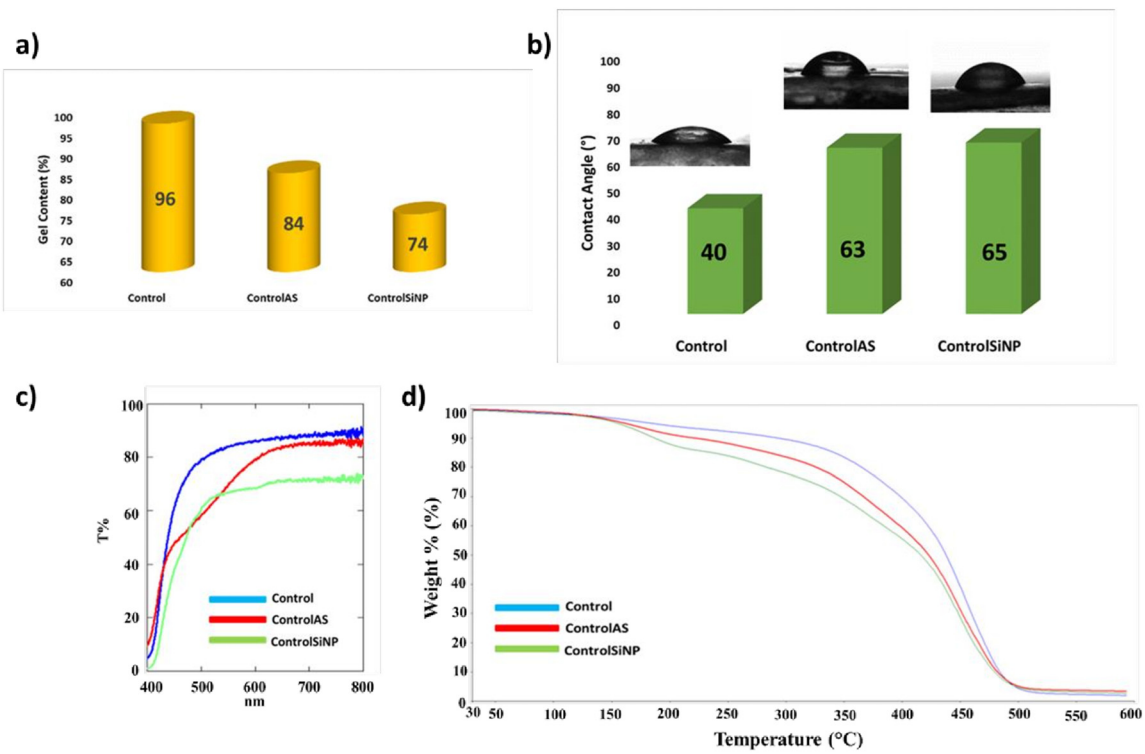

Fig. 18 The gel content values (a), water contact angle values (b), transmission spectra (c), and TGA thermograms (d) of the photosets.

investigated formulations. The char yield of the control sample was 2.2% at 600 °C. However, the char yield slightly increased to 3.5% upon the addition of AS. The addition of silica nanoparticles resulted in a higher char yield (2.9%) than that obtained with the control formulation.

3.4.2. Recycling of the dimer diamine from the photocured films. The biobased monomers used in this work were designed to contain imine groups. It is known that imine functional groups can be hydrolyzed in aqueous acids back to aldehyde/ketone and amine group-bearing former compounds. Based on these properties of imines, many degradable polymers and vitrimers have been prepared.[64–68] Herein, we also attempted to demonstrate that the dimer diamine can be recycled from fully cured films. A small piece (~0.5 g) of a photocured film (ControlAS) was heated to 65 °C in 10 mL of THF/1 M HCl (2 : 8 by volume) for 2 h, according to the literature (Fig. S20).[69] Some portion of the film was dissolved in the mixture. The solution was filtered, and THF was evaporated. 1 M $NaOH_{(aq)}$ solution was added until the pH reached approximately 9. The yellow mixture was extracted with chloroform. Finally, the chloroform was evaporated, and a yellow liquid residue was obtained. The FTIR spectra of the neat diamine dimer and the extracted residue are shown in Fig. S20. It can be seen from the spectrum of the extracted residue that it contains vibration bands similar to the dimer diamine. On the other hand, the spectrum of the residue also displays characteristic vanillin bands, such as the aldehyde carbonyl band (1668 cm^{-1}) and the C–O stretching band at 1026 cm^{-1}. Thus, some of the unreacted bio-based monomers entrapped in the film were also degraded. Therefore, the vanillin residue was also detected. Furthermore, AS could also be extracted into the residue during the THF/HCl treatment. Although the residue is a mixture of vanillin and dimer diamine, vanillin can be removed from the residue by washing with an aqueous solution of sodium bisulfite if necessary.

This result indicates that the films could partially decompose under the above-mentioned conditions, and a residue composed of vanillin and the dimer diamine could be obtained.

3. Conclusion

This paper describes novel synthesized amine compounds and their potential applications in photochemistry. It has been demonstrated that it can be successfully employed in two-component initiator systems in conjunction with an iodonium salt that absorbs up to approximately λ = 320 nm (IOD or HIP) to initiate radical photopolymerization under light-emitting radiation with a wavelength of λ = 340 nm. In addition, it has also been proven that the newly synthesized amine synergist, owing to the presence of a tertiary amine and free thiol groups in its structure, can reduce oxygen inhibition, which is an unfavorable phenomenon characteristic of the radical photopolymerization process. The application of the amine synergist creates new opportunities to replace the current two-component solution. The used of the amine synergist allows the replacement of two independent ingredients, namely an amine (source of additional radicals) and a thiol (reduction of oxygen inhibition), with a single ingredient containing both an amine and a thiol group. In addition, due to the absorption spectrum reaching the UV-A range, the use of the amine synergist allows the expansion of the capabilities of the light sources employed, allowing for greater application possibilities. Most commercially available amines absorb radiation in the ultraviolet range, reaching up to about 350 nm, which does not allow the application of a λ = 365 nm light source. The presence of both groups in a single molecule enables synergistic action, which translates into increased reactivity, selectivity and stability of the system. The employment of a single compound containing an amine group and a thiol group is a more efficient and economical solution than the use of two separate components, which may have important implications for the further development of modern methods of synthesis and chemical applications. Furthermore, it has been proven that the AS compound can be employed in a two-component initiator system in combination with a standard 7MP cationic initiator using light in the visible range. The 7MP initiator, as a one-component initiator system, was insufficient to efficiently initiate radical photopolymerization; when combined with AS, there was a high initiation efficiency. In addition, amine synergists can be utilized in DLP 3D printing, as confirmed by the obtained prints characterized by very high resolution, precision, and surface quality. Another aspect discussed in this article is the synthesis and application of a novel monomer – diamine–vanillin dimethacrylate. The effects of the newly synthesized monomer on the radical photopolymerization kinetics and the DLP 3D printing process were investigated. It has been proven that the addition of a biobased monomer to photocurable resins reduces the induction time. This also proved the suitability of the biobased monomer for obtaining three-dimensional structures with improved mechanical properties. DVDMA bio-based monomers contain imine linkages that are easily cleaved under acidic conditions.

Conflicts of interest

The authors declare that they have no known competing financial interests or personal relationships that could have appeared to influence the work reported in this paper.

Data availability

The data supporting this article have been included as part of the SI.

Supplementary Information includes the following details: (1) description of the synthesis of the amine synergist (AS) compound and its spectroscopic characterization, including analysis by NMR and FT-IR spectroscopy; (2) description of the synthesis and spectroscopic characterization (including NMR

and FT-IR spectroscopy) of the bio-based monomer, dimmer diamine-vanillin dimethacrylate (DVDMA); (3) photolysis measurements of the AS compound in acetonitrile upon irradiation with LEDs at 300 nm, 340 nm, and 365 nm; (4) cyclic voltammetry curves of the amine synergist (AS) in acetonitrile; (5) measurements of the thermal stability of the amine synergist (AS); (6) differential thermal analysis of resin compositions, including Resin-20% BIO-TPO and formulations containing the amine synergist at 1% and 2% concentrations (Resin-20% BIO-TPO-1% AS and Resin-20% BIO-TPO-2% AS); (7) experimental results related to 3D printing of various compositions, including graphics showing 3D models, 2D images, and 3D images of prints obtained with Resin-20% BIO-TPO and Resin-20% BIO-TPO-5% AS; (8) Jacob's working curves for a photocurable resin based on UDMA/HDDA with varying amounts of bio-based monomer and 7 MP initiator; (9) results of 3D printing experiments with compositions based on monomers UDMA/HDDA/BIO, including SEM images of a print obtained with Resin-7MP:AS (1 : 2)_UDMA/HDDA/BIO using DLP technology; (10) results of the recycling process of the dimer diamine from photocured films. See DOI: **https://doi.org/10.1039/d5py00603a**, .

Acknowledgements

This research was financed by the Medical Research Agency under the project 'Onco-Lumi-3D,' No. KPOD.07.07-IW.07-0125/24, from the National Recovery and Resilience Plan (NRRP) program, Component D: Efficiency, Accessibility, and Quality of the Healthcare System, Investment D3.1.1: Comprehensive Development of Research in Medical and Health Sciences. The NRRP program was funded by the European Union Recovery Instrument (NextGenerationEU) through the Recovery and Resilience Facility (RRF) for the period 2021–2026.

References

1 C. Greant, B. Van Durme, J. Van Hoorick and S. Van Vlierberghe, *Adv. Funct. Mater.*, 2023, 33.
2 A. N. Generalova, P. A. Demina, R. A. Akasov and E. V. Khaydukov, *Russ. Chem. Rev.*, 2023, **92**, 2.
3 A. Randhawa, S. D. Dutta, K. Ganguly, D. K. Patel, T. V. Patil and K. T. Lim, *Macromol. Biosci.*, 2023, 23.
4 N. Vidakis, M. Petousis, N. Michailidis, C. David, V. Saltas, D. Sagris, M. Spiridaki, A. Argyros, N. Mountakis and V. Papadakis, *Ceram. Int.*, 2024, **50**, 14919–14935.
5 Y. Qi, H. Lv, Q. Huang and G. Pan, *Eur. Polym. J.*, 2024, **213**, 113133.
6 I. Chiulan, E. B. Heggset, Ş. I. Voicu and G. Chinga-Carrasco, *Biomacromolecules*, 2021, **22**, 1795–1814.
7 S. Enbergs, J. Spinnen, T. Dehne and M. Sittinger, *J. Tissue Eng. Regener. Med.*, 2023, 2023.
8 D. Bahati, M. Bricha and K. El Mabrouk, *Adv. Eng. Mater.*, 2023, 25.
9 I. Roohani, E. Newsom and H. Zreiqat, *Int. Mater. Rev.*, 2023, **68**, 1075–1097.
10 X. Xu, A. Awad, P. Robles-Martinez, S. Gaisford, A. Goyanes and A. W. Basit, *J. Controlled Release*, 2021, **329**, 743–757.
11 I. Seoane-Viaño, S. J. Trenfield, A. W. Basit and A. Goyanes, *Adv. Drug Delivery Rev.*, 2021, **174**, 553–575.
12 Y. Bao, N. Paunović and J. Leroux, *Adv. Funct. Mater.*, 2022, **32**, 2109864.
13 A. Bagheri and J. Jin, *ACS Appl. Polym. Mater.*, 2019, **1**, 593–611.
14 Z. Hu, J. Xu, Y. Wang, L. Xu, Y. Yi, B. Liu and Z. Wang, *ACS Omega*, 2023, **8**, 32396–32403.
15 J. Cao, X. Liu, A. Cameron, J. Aarts and J. J. E. Choi, *J. Mech. Behav. Biomed. Mater.*, 2024, 150.
16 M. Topa-Skwarczyńska, M. Jankowska, A. Gruchała-Hałat, F. Petko, M. Galek and J. Ortyl, *Dent. Mater.*, 2023, **39**, 729–742.
17 Z. Lu, W. Gao, F. Liu, J. Cui, S. Feng, C. Liang, Y. Guo, Z. Wang, Z. Mao and B. Zhang, *Addit. Manuf.*, 2024, **94**, 104443.
18 H. Ding, M. Dong, Q. Zheng and Z. L. Wu, *Mol. Syst. Des. Eng.*, 2022, **7**, 1017–1029.
19 E. Hola and J. Ortyl, *Eur. Polym. J.*, 2021, 150.
20 L. Yao, P. Hu, Z. Wu, W. Liu, Q. Lv, Z. Nie and H. Zhengdi, in *Journal of Physics: Conference Series*, Institute of Physics Publishing, 2020, vol. 1549.
21 X. Wang, J. Liu, Y. Zhang, P. M. Kristiansen, A. Islam, M. Gilchrist and N. Zhang, *Virtual Phys. Prototyp.*, 2023, 18.
22 F. Li, X. Ji, Z. Wu, C. Qi, J. Lai, Q. Xian and B. Sun, *Mater. Lett.*, 2020, **276**, 128037.
23 I. Kamińska, J. Ortyl and R. Popielarz, *Polym. Test.*, 2015, **42**, 99–107.
24 M. Topa, J. Ortyl, A. Chachaj-Brekiesz, I. Kamińska-Borek, M. Pilch and R. Popielarz, *Spectrochim. Acta, Part A*, 2018, **199**, 430–440.
25 D. Nowak, J. Ortyl, I. Kamińska-Borek, K. Kukuła, M. Topa and R. Popielarz, *Polym. Test.*, 2018, **67**, 144–150.
26 J. Ortyl, M. Galek, P. Milart and R. Popielarz, *Polym. Test.*, 2012, **31**, 466–473.
27 J. Ortyl, P. Milart and R. Popielarz, *Polym. Test.*, 2013, **32**, 708–715.
28 J. Ortyl, M. Galica, R. Popielarz and D. Bogdał, *Pol. J. Chem. Technol.*, 2014, **16**, 75–80.
29 J. Ortyl, M. Topa, I. Kamińska-Borek and R. Popielarz, *Eur. Polym. J.*, 2019, **116**, 45–55.
30 M. Topa, E. Hola, M. Galek, F. Petko, M. Pilch, R. Popielarz, F. Morlet-Savary, B. Graff, J. Laleveé and J. Ortyl, *Polym. Chem.*, 2020, **11**, 5261–5278.
31 J. Ortyl, P. Fiedor, A. Chachaj-Brekiesz, M. Pilch, E. Hola and M. Galek, *Sensors*, 2019, **19**, 1668.
32 K. Trembecka-Wójciga, M. Jankowska, W. Tomal, A. Jarzębska, Ł. Maj, T. Czeppe, P. Petrzak, A. Chachaj-Brekiesz and J. Ortyl, *Eur. Polym. J.*, 2023, **198**, 112403.

33 E. Geisler, M. Lecompère and O. Soppera, *Photonics Res.*, 2022, **10**, 1344.
34 J. Jakubiak, X. Allonas, J. P. Fouassier, A. Sionkowska, E. Andrzejewska, L. Å. Linden and J. F. Rabek, *Polymer*, 2003, **44**, 5219–5226.
35 E. Hola, M. Pilch and J. Ortyl, *Catalysts*, 2020, **10**, 1–28.
36 J. W. Park, G. S. Shim, J. H. Back, H. J. Kim, S. Shin and T. S. Hwang, *Polym. Test.*, 2016, **56**, 344–353.
37 V. Jašek, V. Melčová, S. Figalla, J. Fučík, P. Menčík and R. Přikryl, *ACS Appl. Polym. Mater.*, 2023, **5**, 9909–9917.
38 L. Schittecatte, V. Geertsen, D. Bonamy, T. Nguyen and P. Guenoun, *MRS Commun.*, 2023, **13**, 357–377.
39 S. C. Ligon-Auer, M. Schwentenwein, C. Gorsche, J. Stampfl and R. Liska, *Polym. Chem.*, 2016, **7**, 257–286.
40 A. Al Rashid, W. Ahmed, M. Y. Khalid and M. Koç, *Addit. Manuf.*, 2021, 47.
41 S. Luleburgaz, E. Cakmakci, H. Durmaz and U. Tunca, *Eur. Polym. J.*, 2024, 112897.
42 S. A. Begum, P. S. G. Krishnan and K. Kanny, *Polym. Sci., Ser. A*, 2023, **65**(5), 421–446.
43 K. N. A. Putri, V. Intasanta and V. P. Hoven, *Heliyon*, 2024, **10**(4), e25873.
44 H. Zeidler, D. Klemm, F. Böttger-Hiller, S. Fritsch, M. J. Le Guen and S. Singamneni, *Procedia Manuf.*, 2018, **21**, 117–124.
45 P. T. Anastas and J. C. Warner, *Green Chemistry: Theory and Practice*, Oxford University Press, New York, 1998, p. 30.
46 M. Bergoglio, E. Rossegger, S. Schlögl, T. Griesser, C. Waly, F. Arbeiter and M. Sangermano, *Polymers*, 2024, **16**(11), 1510.
47 K. Janssen, G. H. Schnelting, M. Waterink, J. Guit, J. Hul, C. Ye and V. S. Voet, *Macromol. Mater. Eng.*, 2024, 2400036.
48 A. Fantoni, J. Ecker, M. Ahmadi, T. Koch, J. Stampfl, R. Liska and S. Baudis, *ACS Sustainable Chem. Eng.*, 2023, **11**(32), 12004–12013.
49 M. A. El-Tayeb, T. M. Dawoud, K. S. Almaary, F. Ameen and H. A. Khonakdar, *J. Polym. Environ.*, 2025, **33**(1), 358–373.
50 E. Skliutas, M. Lebedevaite, S. Kasetaite, S. Rekštytė, S. Lileikis, J. Ostrauskaite and M. Malinauskas, *Sci. Rep.*, 2020, **10**(1), 9758.
51 V. Schimpf, A. Asmacher, A. Fuchs, K. Stoll, B. Bruchmann and R. Mülhaupt, *Macromol. Mater. Eng.*, 2020, **305**(8), 2000210.
52 X. Chu, J. Tu, H. R. Berensmann, J. J. La Scala and G. R. Palmese, *Polymers*, 2023, **15**(9), 2007.
53 W. Tomal, T. Świergosz, M. Pilch, W. Kasprzyk and J. Ortyl, *Polym. Chem.*, 2021, **12**, 3661–3676.
54 E. Hola, M. Topa, A. Chachaj-Brekiesz, M. Pilch, P. Fiedor, M. Galek and J. Ortyl, *RSC Adv.*, 2020, **10**, 7509–7522.
55 W. Tomal, A. Chachaj-Brekiesz, R. Popielarz and J. Ortyl, *RSC Adv.*, 2020, **10**, 32162–32182.
56 F. Petko, M. Galek, E. Hola, M. Topa-Skwarczyńska, W. Tomal, M. Jankowska, M. Pilch, R. Popielarz, B. Graff, F. Morlet-Savary, J. Lalevee and J. Ortyl, *Chem. Mater.*, 2022, **34**, 10077–10092.
57 M. Jankowska, A. Chachaj-Brekiesz, K. Trembecka-Wójciga, A. Jarzębska, M. Topa-Skwarczyńska, M. Pilch and J. Ortyl, *Polym. Chem.*, 2023, **14**, 2088–2106.
58 F. Petko, E. Hola, M. Jankowska, A. Gruchała-Hałat and J. Ortyl, *Virtual Phys. Prototyp.*, 2023, **18**, 1.
59 W. Tomal, D. Krok, A. Chachaj-Brekiesz, P. Lepcio and J. Ortyl, *Addit. Manuf.*, 2021, **48**, 102447.
60 Z. Altıntaş, E. Çakmakçı, M. V. Kahraman, N. K. Apohan and A. Güngör, *J. Solgel. Sci. Technol.*, 2011, **58**, 612–618.
61 O. Ozukanar, E. Çakmakçi, O. Daglar, H. Durmaz and V. Kumbaraci, *Eur. Polym. J.*, 2023, **195**, 112203.
62 P. Fiedor, M. Pilch, P. Szymaszek, A. Chachaj-Brekiesz, M. Galek and J. Ortyl, *Catalysts*, 2020, **10**, 284.
63 F. Petko, A. Świeży, M. Jankowska, P. Stalmach and J. Ortyl, *Polym. Chem.*, 2023, **14**, 3018–3034.
64 R. Mo, L. Song, J. Hu, X. Sheng and X. Zhang, *Polym. Chem.*, 2020, **11**, 974–981.
65 H. Tran, S. Nikzad, J. A. Chiong, N. J. Schuster, A. E. Peña-Alcántara, V. R. Feig, Y. Q. Zheng and Z. Bao, *Chem. Mater.*, 2021, **33**, 7465–7474.
66 K. Fukuda, M. Shimoda, M. Sukegawa, T. Nobori and J. M. Lehn, *Green Chem.*, 2012, **14**, 2907–2911.
67 J. Stouten, G. H. Schnelting, J. Hul, N. Sijstermans, K. Janssen, T. Darikwa and K. V. Bernaerts, *ACS Appl. Mater. Interfaces*, 2023, **15**(22), 27110–27119.
68 O. Ozukanar, E. Çakmakçi and V. Kumbaraci, *Macromol. Mater. Eng.*, 2024, 2400322.
69 T. Türel and Ž. Tomović, *ACS Sustainable Chem. Eng.*, 2023, **11**, 8308–8316.